

还原性围岩在斑岩钼矿成矿中的作用^{*}

郭东伟^{1,2}, 李延河^{1**}, 段超¹, 范昌福¹, 万秋³, 孙鹏程¹

(1 自然资源部成矿作用与资源评价重点实验室 中国地质科学院矿产资源研究所, 北京 100037; 2 北京大学地球与空间科学学院, 北京 100871; 3 安徽省地质调查院(安徽省地质科学研究所), 安徽 合肥 230001)

摘要 斑岩钼(铜)矿是重要的钼矿资源类型, 高氧逸度岩浆是公认的评价斑岩成矿的有效指标。但前人关注的焦点是成矿母岩浆的起源与演化, 还原性围岩在斑岩成矿中的作用长期被忽视, 是什么触发了高氧化性含矿岩浆热液的还原与成矿还存在不同的认识。文章在前人工作基础上, 以中国秦岭-大别、华北克拉通北缘的南泥湖-三道庄-上房沟、沙坪沟、曹四夭等斑岩型钼矿和美国 Climax-Henderson 巨型斑岩钼矿带中 Mt. Emmons 等斑岩钼矿为例, 重点研究了斑岩钼矿的区域分布与还原性围岩之间的空间关系及成因联系, 探讨了斑岩成矿系统氧化还原状态在成矿过程中的变化及触发机制。笔者发现斑岩钼矿的区域分布明显受黑色含碳质地层和中基性火山岩控制, 在成矿过程中黑色含碳质围岩普遍发生褪色蚀变; 主成矿期矿物流体包裹体中普遍含有甲烷, 蚀变围岩和矿床中热液方解石的 $\delta^{13}\text{C}$ 值普遍较低。因此, 笔者提出含碳质地层和中基性火山岩等围岩中还原性组分的加入是引发斑岩钼(铜)矿成矿系统氧化-还原状态转变和成矿金属沉淀的关键。碳质围岩中有机质热解/碳-水反应产生的甲烷是重要还原剂, CH_4 沿构造裂隙扩散进入斑岩成矿系统, 无需成矿斑岩与围岩直接接触即可将成矿溶液中的 SO_4^{2-} 还原成 S^{2-} , 促使 Mo(Cu) 等成矿元素沉淀富集, 解决了困扰矿床学家多年的一道难题。围岩中碳质含量高, 产生的甲烷浓度高, 在斑岩体内即可将成矿热液中的 SO_4^{2-} 等全部还原, 形成的 Mo(Cu) 矿体主要产在斑岩体及早阶段形成的杂岩体之中; 围岩中碳质含量低, 产生的甲烷数量少, 不足以在岩体内将成矿溶液中 SO_4^{2-} 等全部还原, 剩余的 SO_4^{2-} 等进入围岩后进一步被还原, 钼(铜)矿体则主要赋存于岩体与围岩的内外接触带。含碳质围岩中还原组分在热液阶段加入, 有利于形成大矿富矿。以中基性火山岩为围岩的斑岩钼(铜)矿, 还原剂主要为围岩中的 Fe^{2+} , 成矿溶液中 SO_4^{2-} 被还原的同时, 围岩普遍发生磁铁矿化, 矿体主要产在岩体与围岩接触带。因此, “高氧化性斑岩+还原性富碳质地层/中基性火山岩”是高效评价斑岩能否形成大型 Mo(Cu)矿的新指标。

关键词 高氧逸度; 还原性围岩; 甲烷还原剂; 斑岩钼(铜)矿

中图分类号:P618.42

文献标志码:A

Role of reductive surrounding rocks in formation of porphyry Mo deposits

GUO DongWei^{1,2}, LI YanHe¹, DUAN Chao¹, FAN ChangFu¹, WAN Qiu³ and SUN PengCheng¹

(1 Ministry of Natural Resources Key Laboratory of Metallogeny and Mineral Assessment, Institute of Mineral Resources, Chinese Academy of Geological Sciences, Beijing 100037, China; 2 School of Earth and Space Sciences, Peking University, Beijing 100871, China; 3 Geological Survey of Anhui Province (Anhui Institute of Geological Sciences), Hefei 230001, Anhui, China)

Abstract

Porphyry Mo deposits are the most important type of Mo resource. They result from a high oxygen fugacity of the parent magma, which acts as an effective indicator for evaluating the mineralization. In the ore-forming system of porphyry Mo deposits, sulfur exists mainly as sulfate in highly oxidized magma but as sulfide in ores. What triggers the reduction in the mineralization system that leads to sulfide precipitation has not yet been deter-

* 本文得到国家自然科学基金项目(编号:41973022、41627802、42172102)资助

第一作者简介 郭东伟,男,1989年生,地球化学专业,博士研究生。Email: guodongwei@stu.pku.edu.cn

** 通讯作者 李延河,男,1962年生,地球化学专业,研究员,博士生导师,长期从事矿床同位素地球化学研究。Email: lyh@cei.cn

收稿日期 2023-07-04; 改回日期 2023-08-30。赵海杰编辑。

mined. Most of the previous studies have focused on the origin and evolution of the ore-forming parent magma, and the effects of reductive surrounding rocks on porphyry mineralization have been ignored. In this study, a comprehensive geological-geochemical investigation and review have been performed on the typical porphyry Mo deposits, the Nannihu-Sandaozhuang-Shapingou, and Caosiyao deposits in China, and the Mt. Emmons deposits in America. Black carbonaceous sedimentary layers commonly surround porphyry Mo ores, which are widely altered and discolored during mineralization. CH_4 is commonly present in fluid inclusions in the main mineralization stage, and the $\delta^{13}\text{C}$ values of calcite and fluid inclusions from the altered surrounding rocks and ore deposits are generally low and significantly different from those of marine sedimentary carbonate rocks, indicating that the involvement of reductive components from carbonaceous surrounding rocks might be key to the redox state transformation leading to mineral precipitation. On the other hand, the CH_4 produced by the thermal decomposition of organic matter or carbonaceous reaction with H_2O can diffuse into the ore-forming system along the structural fractures and reduce the SO_4^{2-} in the ore-forming hydrothermal fluids to form sulfide precipitation without direct contact between the intrusion and the carbonaceous surrounding rocks. Moreover, the CH_4 content controls the location of the orebody formation with the high content producing orebodies mainly in the porphyry intrusion and complexes in the early stage, while the low CH_4 content results in the orebodies mainly occurring at the contact zone between the porphyry and carbonaceous surrounding rocks. Compared with the magmatic stage of mineralization, the involvement of reductive components in the carbonaceous surrounding rocks during the hydrothermal stage is more favorable for forming giant/large Mo deposits. The intermediate-basic volcanic rock are another important surrounding rock type of porphyry Mo ores. They provide Fe^{2+} to reduce SO_4^{2-} with widely magnetite alteration during mineralization, and orebodies mainly occur at the contact zone between the porphyry and Fe-rich volcanic rocks. The highly oxidized porphyry with reductive carbonaceous surrounding rocks or Fe-rich volcanic rocks offers a new indicator for efficiently evaluating porphyry Mo mineralization.

Key words: high oxygen fugacity, carbonaceous surrounding rocks, reductive agent CH_4 , porphyry Mo deposits

斑岩型钼矿是重要的钼矿资源类型, 钼金属95%以上来源于斑岩型(+矽卡岩型)矿床(Sillitoe et al., 2010)。世界钼资源分布不均, 全世界约90%的钼分布于中国、美国、智利、秘鲁和加拿大等国家(U.S.G.S., 2023)。传统观点认为斑岩钼矿床的形成与洋壳俯冲密切相关(Sillitoe, 1980), 可划分为裂谷/Climax型(以美国Climax-Henderson钼矿带为典型代表(Seedorff et al., 2004a; 2004b; Ludington et al., 2009))和岩浆弧型(以加拿大Endako(Selby et al., 2000)、MAX(Linnen et al., 1990; Lawley et al., 2010), 美国Quartz Hill、Thompson Creek和Buckingham(Carten et al., 1993)以及秘鲁Tamboras钼矿床(Heintze, 1985)为代表)。中国秦岭-大别钼成矿带则发育于华北克拉通与扬子克拉通碰撞造山后的陆内伸展环境(毛景文等, 1999; 叶会寿等, 2006a; 2006b; Mao et al., 2011; Zhang et al., 2014)。

成矿斑岩常含有岩浆成因石膏, 磁铁矿/赤铁矿等高氧化态矿物(Roedder, 1971; Thomas et al.,

1982; Seedorff et al., 2004a; 2004b; 杨永飞等, 2009a; Yang et al., 2013; 张娟等, 2013; Zhang et al., 2014; Audébat, 2015; Ouyang et al., 2022), 指示初始成矿斑岩岩浆-热液成矿系统具有较高的氧逸度。与斑岩铜矿相比, 斑岩钼矿的氧逸度稍低, 氧逸度:斑岩铜矿>斑岩铜钼矿>斑岩钼矿(Sillitoe et al., 1998; Thompson et al., 1999; Sun et al., 2015)。高氧逸度有利于硫、钼等成矿物质在部分熔融阶段进入熔体, 形成富硫、富钼成矿岩浆; 在岩浆结晶过程中, 高氧逸度有利于富硫、富钼成矿溶液的析出, 因此高氧逸度已成为区分斑岩成矿与否的有效指标(Ballard et al., 2002; Burnham et al., 2012; Muñoz et al., 2012; Trail et al., 2012; Sun et al., 2015; Zhang et al., 2017; Zhou et al., 2018; Gao et al., 2020; 李延河等, 2020; Ouyang et al., 2022; Xu et al., 2023)。高分异、高氧逸度、富水、富硫、富钼等是斑岩成矿的有利因素(Jiang et al., 2021)。但许多斑岩钼矿成矿岩浆具有较低的 $w(\text{Mo})$ (2×10^{-6} ~ 25×10^{-6}) (Audébat, 2015;

Audétat et al., 2017; Ouyang et al., 2020; 2021), 说明成矿物质高效卸载聚集条件可能比岩浆中 Mo 的初始浓度更重要 (Vigneresse et al., 2019)。硫在高氧逸度成矿岩浆中主要以硫酸盐 (SO_4^{2-}) 形式存在, 在矿石中以硫化物形式为主, 说明斑岩岩浆-热液成矿系统氧逸度从早到晚发生了重大转变。什么物质和过程触发了高氧化性岩浆-热液成矿系统氧化-还原状态发生转变, 促使成矿物质高效卸载成矿? 是关系斑岩钼矿成因和高效评价的重大科学问题。李延河等(2020)提出“高氧化性斑岩+还原性富碳质地层/富亚铁火山岩”是评价斑岩铜矿成矿的有效指标, 然而, 前人在斑岩钼矿研究中关注的焦点依旧是成矿母岩的起源与演化, 还原性围岩在斑岩钼矿成矿中作用长期被忽视, 至今尚不清楚。

与斑岩成矿有关的还原性围岩主要有 2 种: ① 黑色富碳质地层; ② 富亚铁火山岩, 主要是中基性火山岩(李延河等, 2020)。在中国斑岩钼矿中还原性碳质地层更发育(李永峰等, 2005; 叶会寿等, 2006a; 向君峰等, 2012; Yang et al., 2017; 陈衍景等, 2020; 李延河等, 2020), 在南美斑岩铜钼矿中富含亚铁的安山质火山岩围岩更普遍(Skewes et al., 2003; Cannell et al., 2005; Stern et al., 2007; Vry et al., 2010)。本文以中国南泥湖-三道庄-上房沟、沙坪沟、曹四夭和美国 Mt. Emmons 等大型-超大型斑岩钼矿为例, 讨论了还原性含碳质地层在斑岩钼矿床成矿中的作用; 以金堆城超大型斑岩钼矿为例, 讨论了还原性中基性火山岩围岩在斑岩钼矿床成矿中的作用。

1 斑岩钼矿床地质特征及其与还原性围岩的关系

大量资料和研究表明, 大型-超大型斑岩钼矿的顶板及周边围岩中普遍存在暗色-黑色还原性含碳质地层和富含亚铁的中基性火山岩。秦岭-大别钼成矿带中的还原性含碳质地层主要为古元古界太华群水底沟组和卢镇关岩群仙人冲岩组黑色含石墨片岩、含石墨片麻岩等(图 1a,b), 新元古界栾川群煤窑沟组、白术沟组和南泥湖组、三川组黑色含碳质片岩、碳质页岩等(图 1c,d), 该成矿带内中基性火山岩为广泛分布的古元古界熊耳群安山质-玄武质火山岩(图 1e,f)(李永峰等, 2005; 叶会寿等, 2006a; 向君峰等, 2012; Yang et al., 2017; 陈衍景等, 2020); 华北克拉通北缘钼成矿带中含碳质地层主要为古元古界集宁群含石墨的片麻岩(王时麒, 1989; 张家辉等,

2019); 北美 Climax-Henderson 钼成矿带含碳质地层主要为白垩系 Mancos 组、Mesaverde 组黑色富含碳质砂岩和泥岩、油页岩及含煤沉积岩层(Donnell, 1961; Roehler, 1979; 1987; Thomas et al., 1982; Sanchez, 1990; Li et al., 2018; Collins, 2020)。

这些黑色还原性含碳质地层的岩性以碳质砂岩、碳质凝灰岩、碳质灰岩等沉积岩系和碳质千枚岩、含石墨片麻岩、含石墨大理岩等变质岩系为主。在部分斑岩钼矿区由于构造隆升剥蚀, 矿床形成时覆盖在斑岩钼矿床上部的还原性含碳质地层已被剥蚀(如美国 Climax、Urad-Henderson 斑岩钼矿), 或仅在矿区外围出露(如鱼池岭斑岩钼矿), 或以残片的形式在矿区及外围零星出露(如沙坪沟斑岩钼矿)。黑色还原性含碳质地层不仅为氧化性斑岩成矿系统提供还原剂, 还是理想的天然隔水层, 是形成大型高品位斑岩钼矿的重要因素和条件。在成矿过程中围岩中有机质热解和/或碳质与热液反应产生的甲烷等还原组分的加入, 引发高氧化性成矿溶液中硫酸盐还原和矿质高效卸载沉淀。斑岩成矿系统中高氧化性成矿溶液与富含亚铁的还原性中基性火山岩反应是引起矿质高效卸载沉淀的另一种重要机制。

为深入了解还原性含碳质地层和中基性火山岩围岩在斑岩成矿中的作用及成因联系, 下面以中国秦岭-大别、华北克拉通北缘和美国 Climax-Henderson 世界上重要的 Mo 成矿带中 5 个典型斑岩钼矿床为例, 简要介绍如下。

1.1 河南栾川南泥湖-三道庄-上房沟斑岩-矽卡岩型钼矿

南泥湖-三道庄-上房沟斑岩-矽卡岩型超大型钼(钨)矿田位于秦岭-大别钼成矿带中段, 栾川矿集区(图 2a), 已查明 Mo 资源储量>200 万 t, W>70 万 t(叶会寿等, 2006a), 包括南泥湖斑岩型钼矿床、三道庄矽卡岩型钼矿床、上房沟斑岩型钼铁矿床等 3 个超大型矿床(李永峰等, 2005), 共同组成举世闻名的南泥湖钼矿田(图 2b)(杨永飞等, 2009b)。南泥湖钼矿田出露的地层主要为中元古界官道口群和新元古界栾川群, 后者分布于矿田中部, 为主要的赋矿地层。栾川群是一套矿区广泛发育的含碳质地层(陈衍景等, 2020), 自下而上可分为 4 个组: ① 白术沟组(Pt_3b)(图 1c,d): 由碳质绢云千枚岩、碳质绢云石英片岩、碳质绢云石英岩夹大理岩组成, 地层厚度~1000 m; ② 三川组(Pt_3s): 下段为变质砂岩夹碳质

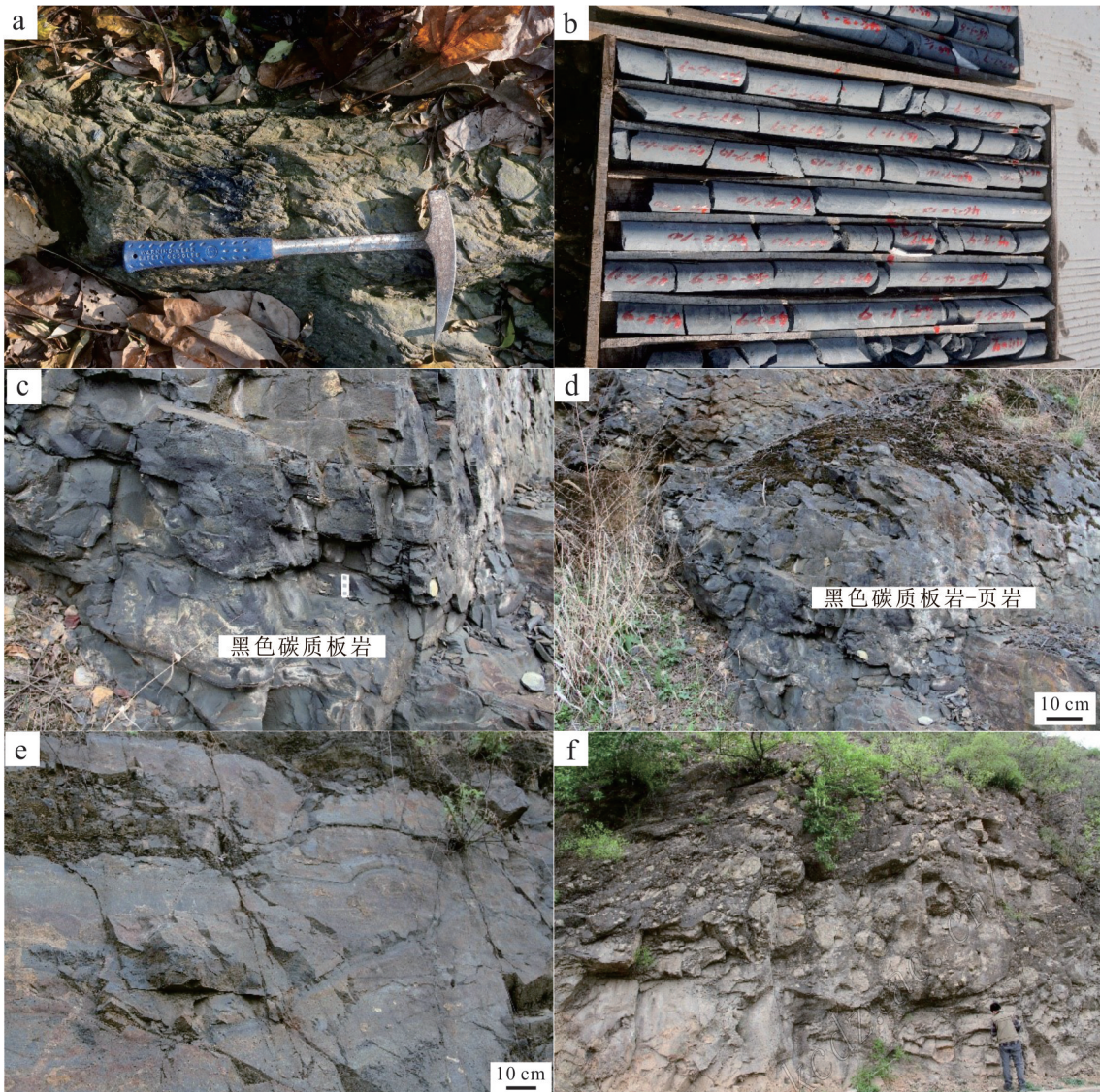


图1 秦岭-大别钼矿带与斑岩钼矿关系密切的黑色还原性含碳质地层和中基性火山岩围岩

a. 沙坪沟钼矿外围卢镇关岩群仙人冲岩组的三和石墨矿地表露头;b. 三和石墨矿岩芯;c. 栾川南泥湖-三道庄钼矿外围栾川群白术沟组厚层状黑色碳质板岩;d. 栾川南泥湖-三道庄钼矿外围栾川群白术沟组黑色碳质板岩;e. 熊耳群鸡蛋坪组玄武安山岩;f. 熊耳群马家河组安山质火山集块岩

Fig.1 Reductive carbonaceous surrounding rocks and intermediate-basic volcanic rocks are closely related to Mo mineralization in the East Qinling-Dabie Mo mineralization belt

a. The surface exposure of the Sanhe graphite deposit occurred in the Xianrenchong Formation of the Luzhenguan Group in the periphery of the Shapinggou Mo deposit; b. Drill cores from the Sanhe graphite deposit; c. The thick-layered black carbonaceous slate of the Baishugou Formation of Luanchuan Group within the boundary of the Nannihu-Sandaozhuang Mo deposits in Luanchuan; d. Black carbonaceous slate of the Baishugou Formation of Luanchuan Group within the boundary of the Nannihu-Sandaozhuang Mo deposits in Luanchuan; e. Basaltic andesite of Jidanping Formation of the Xiong'er Group; f. Andesitic volcanic agglomerate of Majiahe Formation of the Xiong'er Group

千枚岩,上段为大理岩夹钙质片岩,地层厚度471.57 m,为三道庄钼矿床的主要赋矿层位;③南泥湖组(Pt_3n):下段主要为细粒石英岩,中段以变斑二云片岩、碳质绢云片岩及钙质二云片岩为主,地层厚度509 m,是南泥湖斑岩型钼矿床的主要赋矿层位;

④煤窑沟组(Pt_3m):含碳绢云千枚岩、石煤层等,石煤夹层厚度>150 m,地层厚度1100 m,为上房沟斑岩钼矿床的主要赋矿层位。

南泥湖燕山期成矿斑岩体侵入南泥湖地层中。岩体地表呈不规则椭圆状,出露面积近0.12 km²,岩

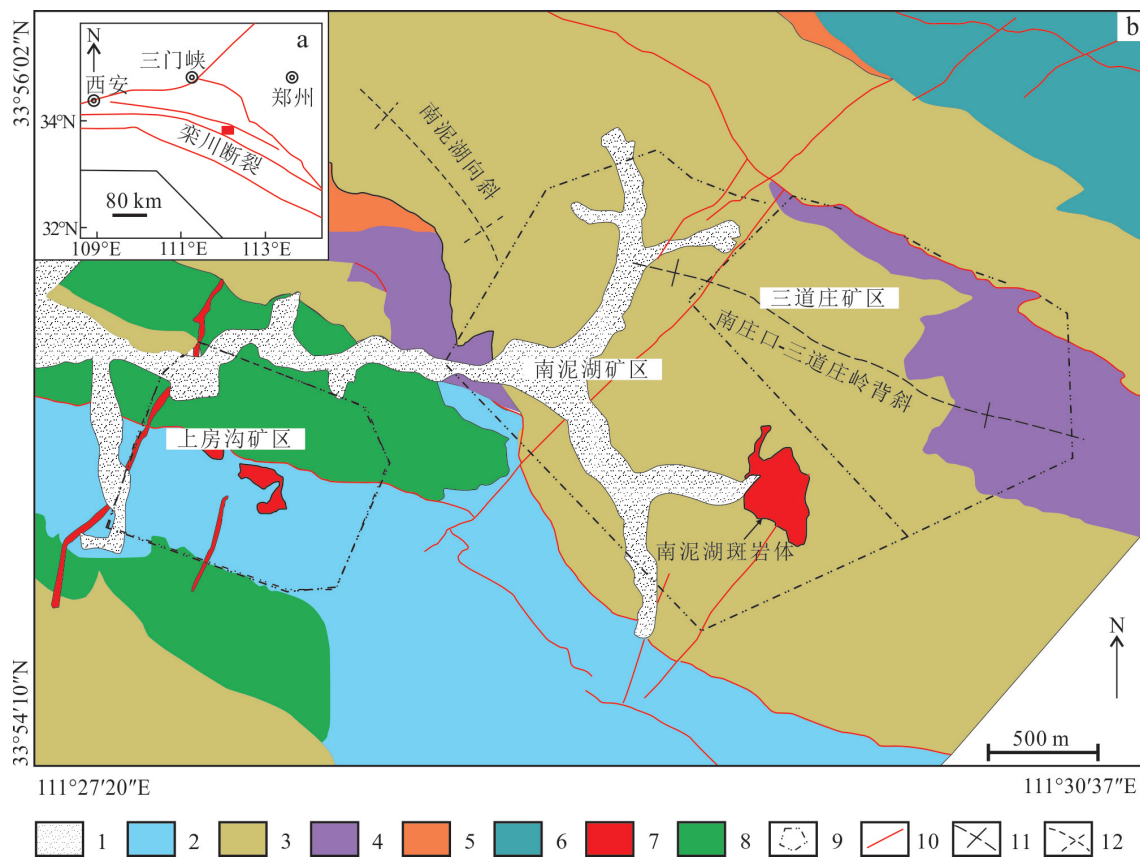


图2 南泥湖钼矿田构造位置简图(a)和地质简图(b,据杨永飞等,2009b)

1—第四纪沉积物;2—栾川群煤窑沟组;3—栾川群南泥湖组;4—栾川群三川组;5—栾川群白术沟组;6—官道口群;7—燕山期花岗岩;
8—加里东期变辉长岩;9—矿区范围;10—断裂;11—背斜;12—向斜

Fig.2 Tectonic location sketch (a) and geological map of the Nannihu Mo field (b, after Yang et al., 2009b)
1—Quaternary sedimentary; 2—Meiyaogou Fm., Luanchuan GP.; 3—Nannihu Fm., Luanchuan GP.; 4—Sanchuan Fm., Luanchuan GP.;
5—Baishugou Fm., Luanchuan GP.; 6—Guandaokou GP.; 7—Mesozoic granite porphyry; 8—Neoproterozoic metagabbro; 9—Deposit
boundaries; 10—Fault; 11—Anticline; 12—Syncline

体深部变大。岩体浅部为斑状二长花岗岩,向深部逐渐过渡为斑状黑云母花岗闪长岩。南泥湖矿区钼矿体赋存于南泥湖斑岩体内部及其外接触带的黑云母长英角岩中(图3)。三道庄矿区钼矿体主要赋存于三川组上段由接触变质和交代作用形成的钙硅酸盐角岩和矽卡岩中,主矿体形态简单,呈厚层状,在矿区范围内长度大于1420 m,厚度80~150 m,最大厚度可达364 m(图3)(杨永飞等,2009b)。上房沟钼铁矿钼矿化位于花岗斑岩体内部、接触带矽卡岩及蚀变辉长岩中(Yang et al., 2013)。矿田金属矿物主要为黄铁矿、辉钼矿、磁铁矿、磁黄铁矿、白钨矿、黄铜矿等。热液蚀变强烈、类型复杂,由岩体向外表现出一定的分带性:①钾化、②硅化、③绢英岩化、④矽卡岩化、⑤阳起石

化、⑥碳酸盐化、⑦萤石化。成矿过程分为4个阶段:阶段Ⅰ,为硅化、钾化和矽卡岩化,发育少量磁铁矿、辉钼矿;阶段Ⅱ,为主要的钼矿化阶段,硅化、绢英岩化强烈,以大量发育石英-钾长石-辉钼矿脉、石英-辉钼矿脉、石英-硫化物脉、薄膜辉钼矿脉为特征;阶段Ⅲ,为多金属硫化物矿化,以发育黄铁矿脉、石英-硫化物-碳酸盐脉为特征;阶段Ⅳ,以发育碳酸盐脉、石英-碳酸盐脉、碳酸盐-萤石脉为特征,基本不含硫化物。上房沟钼铁矿床,阶段Ⅰ矿物流体包裹体以H₂O-CO₂包裹体为主,常见纯CO₂包裹体,子矿物为磁铁矿等,显示相对氧化环境特征,阶段Ⅱ、阶段Ⅲ,矿物流体包裹体除CO₂和/或H₂O外,含少量CH₄、CO还原性气体组分,显示相对还原特征(Yang et al., 2013)。

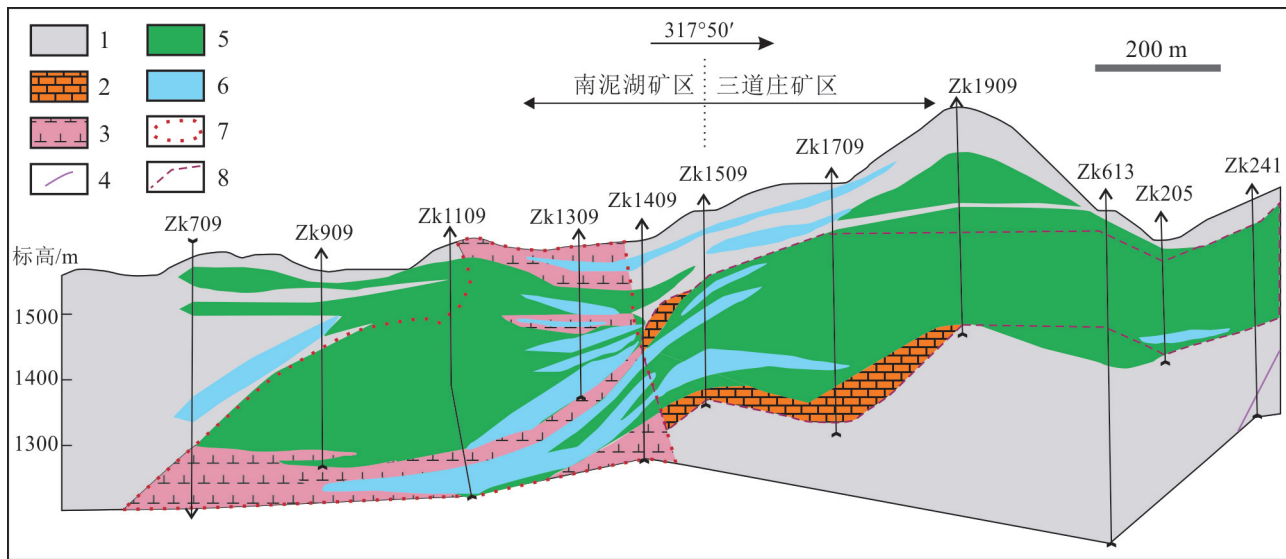


图3 南泥湖-三道庄钨钼矿床横9线勘探剖面图(据杨永飞等,2009b)

1—各类角岩;2—矽卡岩;3—花岗斑岩;4—断裂构造;5—表内矿体;6—表外矿体;7—斑岩体边界;8—矽卡岩边界

Fig.3 Geological section along No. 9 exploration line in Nannihu-Sandaozhuang W-Mo deposit(after Yang et al., 2009b)

1—Hornfels; 2—Skarn; 3—Granite porphyry; 4—Fault; 5—High-grade Mo orebody; 6—Low-grade Mo orebody; 7—Porphyry bodudary;
8—Skarn boundary

1.2 安徽金寨沙坪沟斑岩型钼矿

沙坪沟斑岩型钼矿床位于大别造山带东段,已探明钼金属储量230万t,平均品位>0.1%(张怀东等,2012),为世界第二大钼矿床,该区出露地层主要为元古界卢镇关岩群的变火山-沉积岩,岩性主要为黑云斜长片麻岩、二长片麻岩、斜长角闪片麻岩和变粒岩、大理岩、云母片岩、石墨片岩等。在金寨铁冲乡皂河一带卢镇关岩群仙人冲岩组中段石墨云母石英片岩、石墨红柱石千枚岩等富集形成石墨矿床(图1a、b)。由于受到燕山期强烈的岩浆构造作用的影响,沙坪沟钼矿床形成后,该地区地壳发生了隆升,遭受了风化剥蚀,使卢镇关岩群呈残留体和捕虏体出露于沙坪沟矿田的西部和北部(图4)(陆三明等,2019),使形成于数公里之下的斑岩钼矿床逐渐接近于地表,花岗斑岩体正上部的青磐岩化带、泥化带以及脉型Pb-Zn矿体已被全部剥蚀破坏,只保留下了岩体周边的青磐岩化带、脉型Pb-Zn矿体,而斑岩钼矿主体基本未受剥蚀(何俊等,2016;任志等,2020)。钼矿体主要赋存于隐伏花岗斑岩体与正长岩(围岩)的接触带内。

沙坪沟钼矿床的主矿体只有1个,呈筒状产出,厚度大,矿化连续。众多的零星小矿体围绕主矿体两侧分布。外围多个铅锌矿床(点)以沙坪沟

钼矿床为中心呈环形分布,矿体明显受断裂控制。围岩蚀变发育,从花岗斑岩体向外,划分为3个蚀变带:(I)钾(钠)长石-硅化带→(II)黄铁绢英岩化带→(III)绿泥石-碳酸盐化带。成矿过程划分为4个阶段:①钾(钠)长石-石英-磁铁矿/赤铁矿阶段,含少量辉钼矿和黄铁矿,矿化弱,铁氧化物呈浸染状分布;②石英-钾长石-辉钼矿阶段,为辉钼矿的主成矿阶段,石英-(黄铁矿)-辉钼矿细脉、网脉在岩体与围岩接触带中广泛发育;③黄铁绢英岩化阶段,以大量黄铁矿化、绢云母化、硅化为主要特征,而辉钼矿化减弱;④石英-萤石-石膏阶段,以出现大量石英-萤石为主要特征,在该矿区的北东侧形成了小型萤石矿床,石膏脉比较发育(图5a~f)。矿物共生组合指示成矿系统氧逸度从岩浆-热液期到主成矿期有逐渐降低的趋势,至成矿晚期又有所升高。

1.3 内蒙古兴和曹四夭斑岩型钼矿床

内蒙古兴和县曹四夭斑岩钼矿床位于华北克拉通北缘钼成矿带,已探明钼金属量175.6万t。在斑岩型钼矿床的外围和上部发育热液脉型铅锌金矿床(图6)。区内前寒武系变质岩系广泛出露,主要包括古元古界兴和群、集宁群(张家辉等,2019)。集宁群黄土窑岩组主要分布于矿区中部,为曹四夭斑岩钼矿的赋矿围岩,主要岩性有夕线石石榴子石钾长片

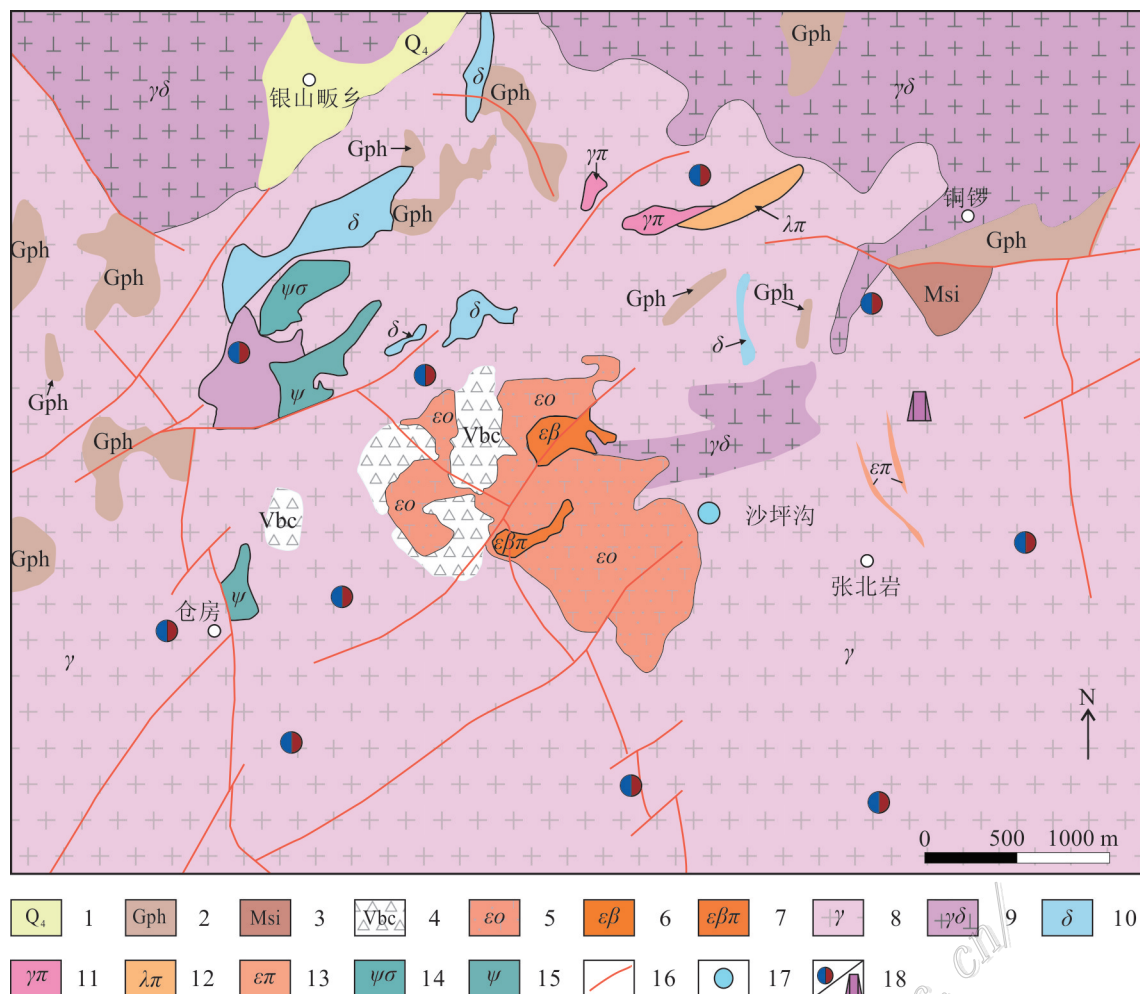


图4 沙坪沟钼矿床平面地质图(据陆三明等,2019)

1—第四系;2—卢镇关群角闪斜长片麻岩;3—硅质大理岩;4—爆发角砾岩;5—石英正长岩;6—黑云母正长岩;7—黑云母正长斑岩;
8—花岗岩;9—花岗闪长岩;10—闪长岩;11—花岗斑岩;12—石英斑岩;13—正长斑岩;14—角闪辉石岩;15—辉石岩;16—断层;
17—钼矿;18—铅锌矿/萤石矿

Fig.4 Geological map of the Shapinggou Mo deposit (Modified from Lu et al., 2019)

1—Quaternary; 2—Amphibole plagiogneiss of Luzhenguan Group; 3—Siliceous marble; 4—Explosion breccia; 5—Quartz syenite; 6—Biotite syenite; 7—Biotite orthophyre; 8—Granite; 9—Granodiorite; 10—Diorite; 11—Granite porphyry; 12—Quartz porphyry; 13—Orthophyre; 14—Hornblende pyroxenite; 15—Pyroxenite; 16—Fault; 17—Molybdenum ore; 18—Lead-zinc/Fluorite ore

麻岩、夹石榴子石黑云斜长片麻岩、含石墨片麻岩、混合岩及透辉大理岩等。集宁群发育厚约300 m的含石墨夹层,是内蒙古中部石墨矿床的重要赋存层位,产出多个大型石墨矿床(王时麒,1989;杨彪等,2023)。中生界主要为中侏罗统陆相碎屑岩,上侏罗统零星分布,主要为安山岩和凝灰岩。矿区内与钼成矿有关的燕山期正长花岗斑岩呈岩株状产出,LA-ICP-MS锆石U-Pb成年龄为148.5~149.9 Ma(Wu et al., 2016; Wu et al., 2017)。辉钼矿的Re-Os等时线年龄和加权平均年龄分别为(148.3 ± 1.3) Ma和

(148.5 ± 1.1) Ma。曹四夭钼矿体主要产于晚侏罗世正长花岗斑岩与集宁群黄土窑岩组斜长浅粒岩和含石墨黑云石榴斜长片麻岩的外接触带, 少量产在内接触带(图6)。

矿床主要金属矿物为辉钼矿和黄铁矿,其次为磁铁矿、黄铜矿和磁黄铁矿及少量黑钨矿。脉石矿物主要为石英和绢云母,其次为钾长石、黑云母、白云母、绿帘石、萤石和方柱石。曹四夭钼矿床具有典型斑岩钼矿床的围岩蚀变类型及分带特征,钾化带规模较小,仅出现在花岗斑岩体的顶部,并伴生少量

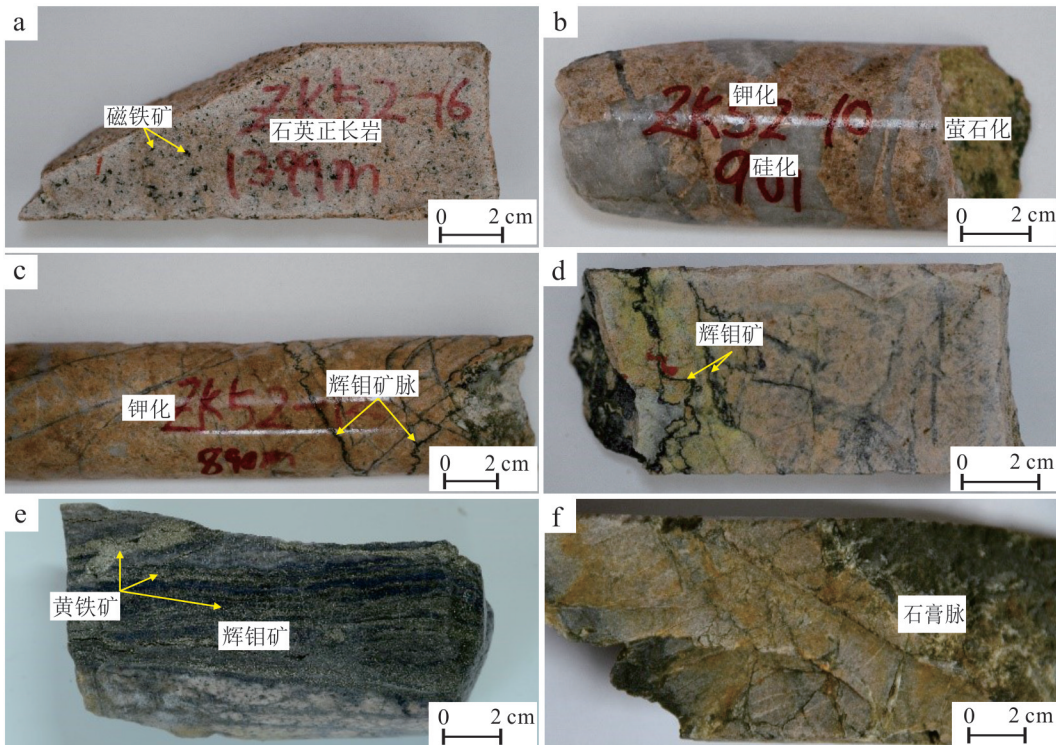


图5 沙坪沟斑岩钼矿床矿石特征

a. 矿床深部新鲜石英正长岩富含原生磁铁矿; b. 钾化→硅化→萤石化(从早到晚); c. 钾化和网脉状辉钼矿化; d. 锯齿状辉钼矿沿裂隙充填; e. 晚期黄铁矿交代早期辉钼矿; f. 成矿晚期沿裂隙充填的白色石膏脉

Fig.5 Photographs of ore features in the Shapinggou porphyry Mo deposit

a. Primitive magnetite developed in fresh quartz syenite from deep deposits; b. Potassium alteration, silicification, and fluoritization from the early to late stages; c. Potassium alteration and vein of molybdenite mineralization; d. Sawtooth-shaped molybdenite filled in the fissures; e. Later pyrite replaced earlier molybdenite; f. White gypsum veins filled in the fractures in the late stage

钼矿体;绢英岩化带产于钾质蚀变带的外围,规模最大,主要的钼矿体均产于该蚀变带中;泥化带叠加于绢英岩化带之上;青盘岩化带位于蚀变带的最外侧,以集宁群变质岩中出现少量绿泥石化、绿帘石化和方解石化为标志,该蚀变带中未见钼矿化(图6)(Wu et al., 2016; Wu et al., 2017)。成矿分为3阶段:①石英+辉钼矿±磁铁矿±黄铁矿阶段、②辉钼矿+黄铁矿±磁黄铁矿±黄铜矿阶段和③石英+方解石+萤石阶段。

1.4 Mt. Emmons 斑岩型钼矿床

Mt. Emmons 斑岩型钼矿田位于太平洋东岸北美Colorado(Climax-Henderson)钼成矿带中部,该成矿带发育Urad-Henserson、Climax、Mt. Emmons、Silver Creek等多个世界级斑岩型钼矿床(图7a)。Mt. Emmons 矿田包含位于Redwell盆地下部的上Redwell矿床和下Redwell矿床,以及Red Lady盆地西缘的Mt. Emmons钼矿床(图7b)。白垩纪Mancos

组、Mesaverde组沉积岩在矿区广泛分布,岩性主要为黑灰色层状海相碳质泥页岩,包含粉砂岩、砂岩和砂质灰岩等(Lorenz et al., 2002)。古近纪的Ohio Creek组和Wasatch组砾岩砂岩层覆盖其上(图7b)。Redwell花岗斑岩体向上侵入至Mancos组、Mesaverde组含碳质地层,接触部位形成含黄铁矿、磁黄铁矿的角岩带,靠近岩体300 m厚深棕色角岩带发生褪色蚀变,之上为150 m厚黑色角岩带(Thomas et al., 1982)。Redwell矿床矿体赋存于Redwell斑岩体与围岩角岩接触蚀变带,下部矿体位于Redwell斑岩体内,Mt. Emmons矿床矿体位于角岩接触带。从岩体向外蚀变带依次为钾化带(石英、磁铁矿和黑云母),绢英岩带(石英、绢云母和黄铁矿)和青磐岩化带。矿石矿物包括辉钼矿、黄铁矿、磁黄铁矿、石英、绿帘石、绿泥石和方解石等。

位于该成矿带的Climax和Urad-Henderson超大型斑岩钼矿床与Mt. Emmons斑岩型钼矿床地质特

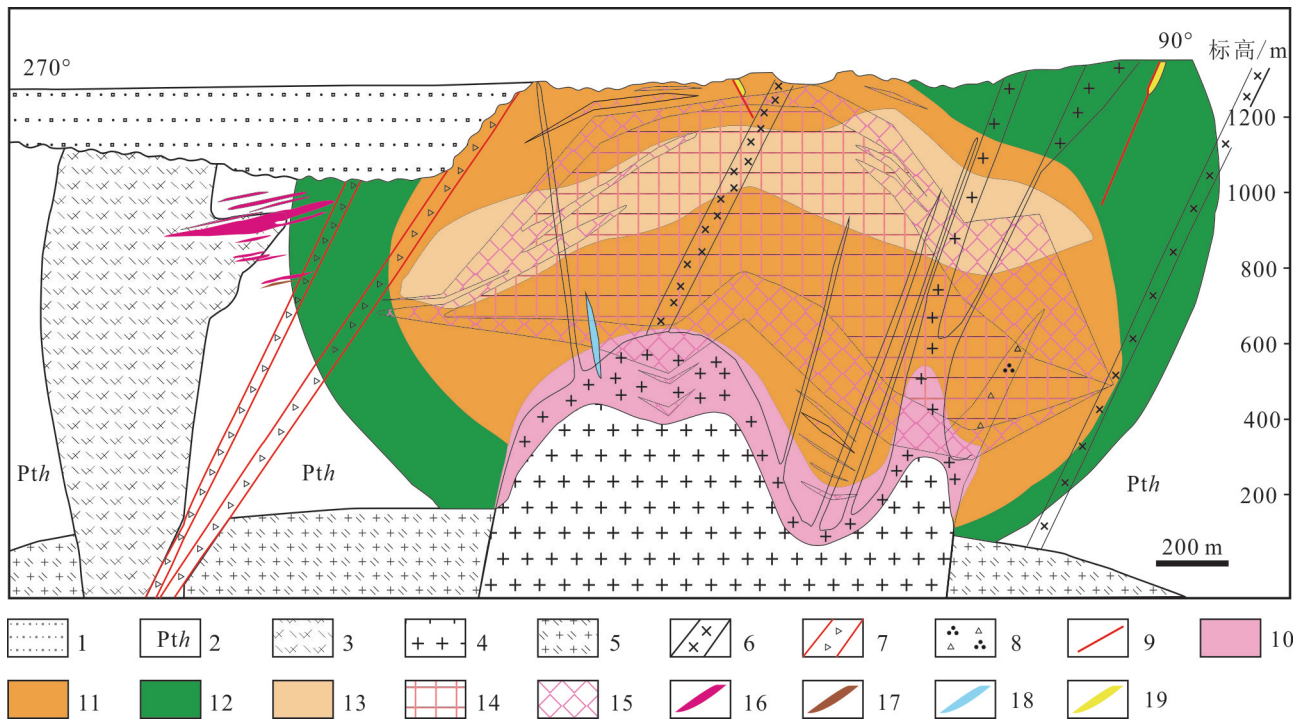


图6 曹四夭斑岩钼矿横08勘探线剖面图(据河南省地质矿产开发局第二地质勘查院,2014修改)
1—新生界沉积物;2—古元古界集宁群黄土窑组变质岩;3—早白垩世角砾状流纹斑岩;4—晚侏罗世正长花岗斑岩;5—晚侏罗世二长花岗岩;6—新元古代辉绿岩脉;7—断裂破碎带;8—隐爆角砾岩;9—断裂;10—钾化带;11—绢英岩化带;12—青磐岩化带;13—泥化带;14—工业钼矿体;15—低品位钼矿体;16—铅锌矿体;17—铅锌金矿体;18—铅金矿体;19—金矿体

Fig. 6 Geological transverse-section along No. 08 exploration of the Caosiyao porphyry Mo deposit (modified after No. 2 Geoexploration Party, Henan Bureau of Geoexploration and Mineral Development, 2014)

1—Quaternary sediments; 2—Huangtuya Formation metamorphic rocks of the Palaeoproterozoic Jining Group; 3—Early Cretaceous brecciated rhyolite porphyry; 4—Late Jurassic syenogranite porphyry; 5—Late Jurassic monzogranite; 6—Neoproterozoic diabase dike; 7—Broken fault zone; 8—Crypto explosive breccia; 9—Fault; 10—Potassic alteration zone; 11—Silicification-sericitization zone; 12—Propylitization zone; 13—Argillization zone; 14—Mo orebody; 15—Mo mineralized orebody; 16—Pb-Zn orebody; 17—Pb-Zn-Au orebody; 18—Pb-Au orebody; 19—Au orebody

征和成矿时代相似,矿体直接赋存于Silver plume花岗岩岩体之中(Clark, 1972; Seedorff et al., 2004a; 2004b)。在Climax和Urad-Henderson等超大型钼矿床附近,Mesaverde组和Wastch组中发现可开采的天然气储量达 2.4×10^{13} 立方英尺(Drake et al., 2019),天然气主要源自Mesaverde组煤层及碳质页岩。Wastch组、Mesaverde组黑色碳质泥页岩、泥砂岩在区域上是重要的烃源岩,同时为斑岩钼成矿提供了还原剂和良好的隔水层。Climax和Urad-Henderson等斑岩钼矿区未见Wastch组、Mesaverde组合含碳质围岩,可能与地壳抬升,沉积地层被剥蚀有关。

斑岩钼矿区及附近发育黑色含碳质地层是非常普遍的地质现象,斑岩钼矿的区域分布明显受黑色含碳质地层控制。虽然有些斑岩钼矿区缺失含碳质

地层(如中国的鱼池岭、沙坪沟钼矿,美国的Climax和Urad-Henderson钼矿等),但其附近分布的石墨矿、煤层或天然气气藏指示斑岩钼矿形成时存在的含碳质地层可能因地壳隆升被剥蚀破坏。含碳质围岩为氧化性成矿流体提供还原剂,使成矿流体中硫酸盐还原形成辉钼矿等矿石矿物,是形成大型高品位斑岩钼矿的重要条件。

1.5 陕西华县金堆城斑岩钼矿

陕西省华县金堆城斑岩钼矿床位于秦岭-大别钼成矿带的西端,已探明Mo资源储量97.8万t,平均品位0.099%,达超大型规模(王晓霞等,2015;陈衍景等,2020)。矿区内地层主要为熊耳群和官道口群(图8a)。熊耳群岩性主要为安山岩和玄武安山岩,含少量流纹岩类、凝灰岩。官道口群高山河组分布于矿区南部,沿碌碡沟断裂不整合覆盖于熊耳群火

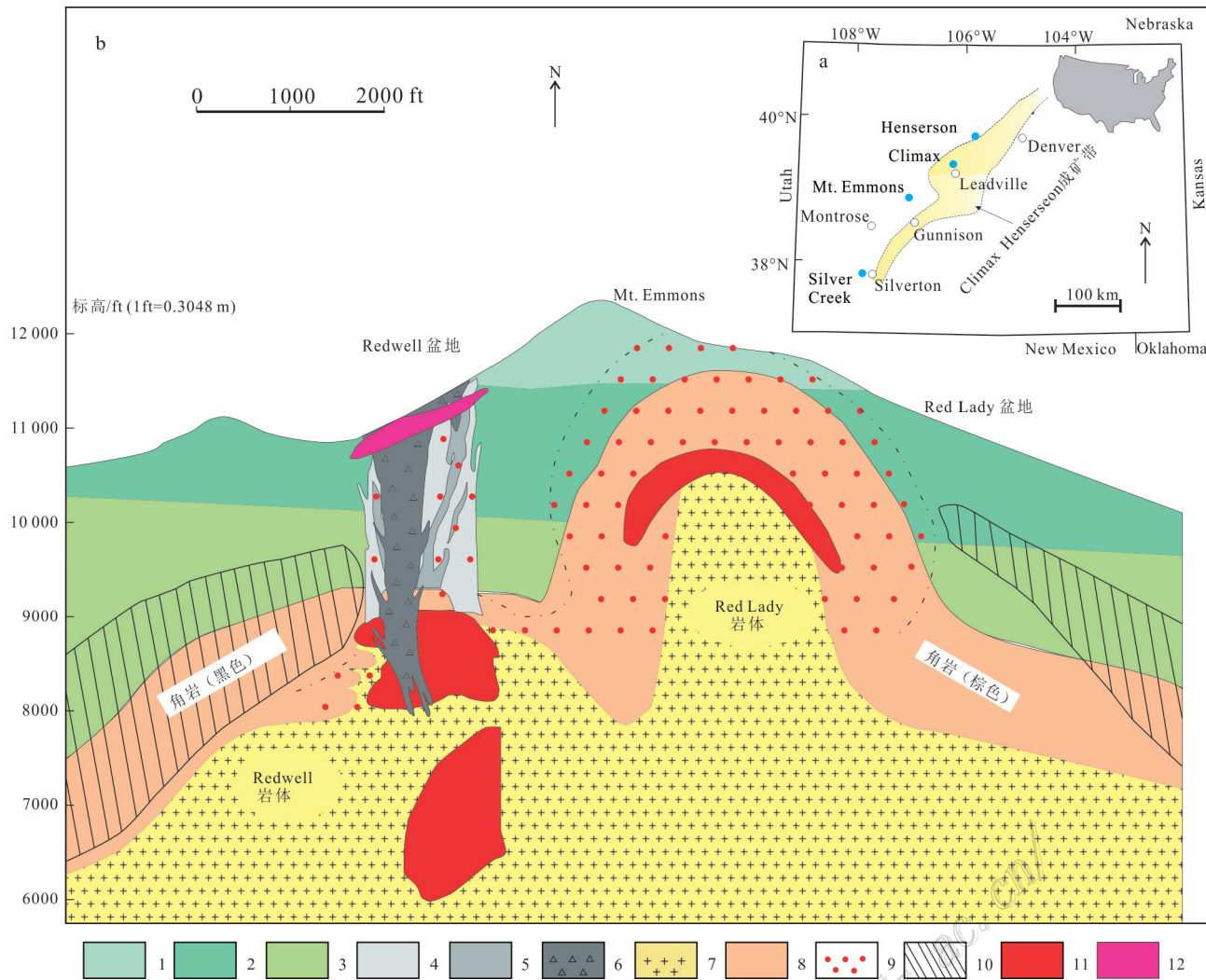


图 7 Colorado 成矿带以及 Urad-Henderson, Mt. Emmons, Silver Creek 斑岩型钼矿床位置(a)和 Mount Emmons 斑岩型钼矿剖面图(b, 据 Audetat et al., 2017 修改)

1—Wastch 组和 Ohin Creek 组; 2—Mesaverde 组; 3—Mancos 组; 4—长英质岩; 5—火成角砾岩; 6—爆破角砾岩; 7—花岗斑岩; 8—角岩;
9—绢英岩化; 10—磁黄铁矿化; 11—Mo 矿体; 12—Zn+Pb+Cu 矿体

Fig.7 Map of Colorado showing the locations of the Urad-Henderson, Mt. Emmons and Silver Creek porphyry Mo deposits and the outlines of the Colorado Mineral Belt (a) and schematic cross-section through the porphyry Mo deposits in the Redwell Basin and Mt. Emmons, Colorado, in America (b, modified from Audetat et al., 2017)

1—Wastch and Ohin Creek Fm.; 2—Mesaverde Fm.; 3—Mancos Fm.; 4—Felsite; 5—Igneous breccia; 6—Rubble breccia; 7—Granite porphyry;
8—Horfels; 9—Phyllitic alteration; 10—Pyrrhotite; 11—Mo orebody; 12—Zn+Pb+Cu orebody

山岩之上,为滨海-浅海相碎屑岩沉积建造。自下而上可分为3个岩性段:下段为紫红色砾岩、粉砂岩,灰白色石英岩夹变石英砂岩和泥板岩;中段为变石英砂岩夹泥质板岩;上段为厚层紫红-灰白色石英岩夹变石英砂岩。金堆城花岗斑岩体呈岩枝状侵入于熊耳群玄武安山岩中,地表出露长400 m,宽150 m,面积0.067 km²(图8a)。金堆城花岗斑岩体形成于141 Ma(朱赖民等,2008;郭波等,2009),金堆城钼矿

床辉钼矿 Re-Os 同位素年龄为 139 Ma(黄典豪等,1994),略晚于金堆城花岗斑岩的侵位年龄。

金堆城钼矿体以金堆城花岗斑岩为中心赋存于岩体内部及其内外接触带中(图8b),矿体呈一连续扁豆体状展布,地表出露长约 1600 m,深部钻孔控制长度约 2200 m,厚 600~700 m,钼矿化由岩体向四周逐渐减弱。金堆城钼矿矿石类型以安山岩型为主(70%),花岗斑岩型次之(25%),石英岩型少量

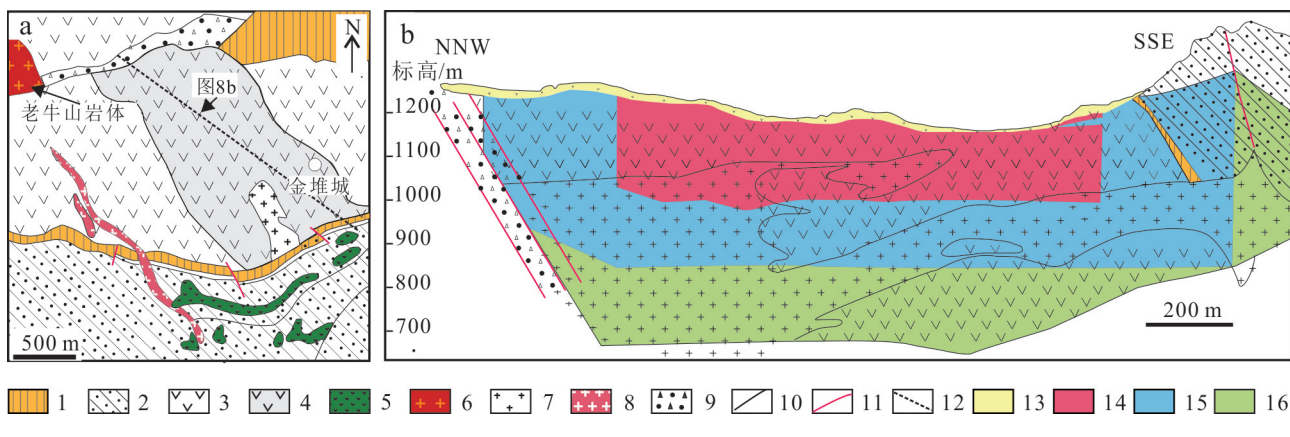


图8 金堆城钼矿床地质略图(a)及9号勘探线剖面图(b)(据Mao et al., 2011)

1—中元古界官道口群板岩;2—中元古界官道口群石英岩;3—中元古界熊耳群安山岩;4—黑云母化安山岩;5—辉绿岩;6—老牛山杂岩;
 7—金堆城花岗斑岩;8—燕山期花岗岩;9—断裂破碎带;10—地质界线;11—断裂;12—勘探线;13—氧化钼矿体(0.087%~0.352%);
 14—钼矿体(0.084%~0.157%);15—钼矿体(0.091%~0.709%);16—钼矿体(0.079%~0.096%)

Fig. 8 Geological map (a) and No. 9 exploration profile (b) of the Jinduicheng porphyry Mo deposit (after Mao et al., 2011)

1—Neoproterozoic slate of Guandaokou Group; 2—Neoproterozoic quartzite of Guandaokou Group; 3—Mesoproterozoic andesite rocks of Xiong'er Group; 4—Biotite andesite; 5—Diabase; 6—Laoniushan complex; 7—Jinduicheng granite porphyry; 8—Yanshanian granites; 9—Fault zone; 10—Geological boundaries; 11—Fault; 12—Exploration line; 13—Oxidized Mo orebody grade (0.087%~0.352%); 14—Mo orebody grade (0.084%~0.157%); 15—Mo orebody grade (0.091%~0.709%); 16—Mo orebody grade (0.079%~0.096%)

(5%)。矿石矿物以辉钼矿和黄铁矿为主,其次为黄铜矿、方铅矿、闪锌矿和磁铁矿;脉石矿物主要为钾长石、斜长石、石英、黑云母,其次为绢云母、白云母、萤石、绿帘石、方解石等。磁铁矿等铁氧化物在安山岩型和花岗斑岩型矿石中更发育。金堆城钼矿床具典型斑岩型钼矿床围岩蚀变特征,自斑岩体向外呈现有规律的面型蚀变:①钾化,②绢英岩化,③硅化,④青磐岩化,⑤碳酸盐化。根据矿物共生组合、矿石组构及脉体穿插关系,将成矿过程分为早、中、晚3个阶段:①早阶段以发育钾长石脉、钾长石-石英±黄铁矿脉、石英脉为特征,硫化物较少;②中阶段以发育石英-硫化物±钾长石网脉、石英-辉钼矿脉、石英-硫化物±萤石±方解石网脉、多金属硫化物网脉为特征,为钼矿化的主要阶段;③晚阶段以出现低温的绿泥石和方解石为特征,主要发育无矿石英脉、石英-萤石-碳酸盐脉、石英-碳酸盐脉,基本不含硫化物。金堆城钼矿床各成矿阶段脉石矿物中流体包裹体类型丰富,形态多样。主要类型有4类:①纯CO₂包裹体(PC型),主要存在于早-中阶段石英脉中;②CO₂-H₂O型包裹体(C型),在早、中阶段热液石英中大量发育;③水溶液包裹体(W型),成矿各阶段均有发育;④含子晶多相包裹体(S型),多见于早、中阶段石英中,子矿物有赤铁矿、黄铜矿、方解石和石膏。

2 讨 论

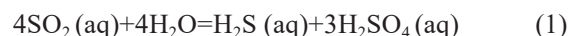
2.1 氧化-还原状态转换是斑岩成矿关键环节

高氧化性斑岩是形成斑岩钼(铜)矿的必要条件,但并不是所有的氧化性斑岩都能成矿。斑岩成矿不仅需要将S、Mo(Cu)等成矿物质从岩浆-热液系统以溶液形式析出,还需要将溶液中的S、Mo(Cu)等成矿物质以金属硫化物的形式在矿体圈闭位置高效沉淀富集起来(Wilkinson, 2013)。如前所述,硫在高氧化性岩浆中主要以SO₄²⁻形式存在,在斑岩钼(铜)矿中主要以硫化物形式存在,表明成矿过程硫的氧化-还原状态发生了重大转变。这已被一系列地质现象研究所证实,如沙坪沟斑岩型钼矿床,成矿斑岩中锆石的Ce⁴⁺/Ce³⁺和Eu/Eu*比值普遍较高,指示成矿斑岩具有高氧化性特征(张红, 2011),新鲜成矿斑岩富含原生磁铁矿,在早期高温钾硅酸盐化成矿阶段钼矿化较弱,矿物组合以含磁铁矿、赤铁矿和硬石膏等高氧化性矿物组合为特征,含子晶多相包裹体中见赤铁矿子晶,指示成矿系统氧逸度较高;中期中高温钾化-石英化-辉钼矿化-黄铁绢英岩化阶段为主成矿期,主要矿物为辉钼矿、黄铁矿等还原性矿物,不见磁铁矿、硬石膏等高氧化性矿物,指示成矿系统氧逸度下降;在成矿晚期,出现绿泥石-石英-萤石-石

膏-碳酸盐组合,指示成矿系统氧逸度又升高(陆三明等,2019;任志等,2020)。南泥湖-三道庄钼钨矿床早期成矿阶段发育磁铁矿、赤铁矿等高氧化性矿物,早期成矿流体明显富K⁺、CO₂和SO₄²⁻,指示成矿系统氧逸度较高;中期主成矿阶段成矿流体富含CH₄、H₂S和CO,盐度显著增加,硫化物大量沉淀,指示成矿流体发生了沸腾,成矿系统氧逸度降低;成矿阶段晚期成矿流体基本不含还原性气体,硫化物矿化微弱,说明成矿系统氧逸度又升高(刘孝善等,1987;石英霞等,2009;陈衍景等,2020)。上房沟钼矿床阶段Ⅰ石英斑晶内的包裹体气相成分以CO₂和H₂O为主,子矿物出现磁铁矿、赤铁矿等,说明阶段Ⅰ为氧化环境;主成矿阶段Ⅱ、Ⅲ石英包裹体内主要为CO₂和H₂O,含少量CH₄和CO,显示阶段Ⅱ、Ⅲ为还原环境(Yang et al., 2013)。曹四夭斑岩钼矿早期成矿阶段富含磁铁矿,中期主成矿阶段富含磁黄铁矿,指示成矿系统氧逸度从早到晚有逐渐降低的趋势(范海洋等,2018)。金堆城钼矿床早阶段流体包裹体含赤铁矿子晶等,指示早阶段成矿流体氧逸度较高,中阶段流体包裹体含黄铜矿等子矿物指示氧化性流体呈还原性,晚阶段成矿流体基本不含还原性气体,硫化物矿化微弱,指示成矿系统氧逸度升高。

关于斑岩成矿系统氧化-还原状态转变的原因,目前主要有以下3种不同认识:①磁铁矿结晶:Wilkinson(2013)和Sun等(2013; 2015)认为岩浆中磁铁矿结晶析出是造成岩浆-热液成矿系统氧化-还原状态转变的主要原因。Richards(2015)持不同观点,指出在相对氧化的斑岩岩浆中,磁铁矿结晶不仅不能使岩浆f(O₂)的降低,反而使残余岩浆f(O₂)的升高。②SO₂脱气:SO₂脱气被认为是造成岩浆-热液系统氧化还原状态转变的原因之一(Kelley et al., 2012)。Richards(2015)认为,在典型富硫、中等氧化的弧岩浆中SO₂脱气将造成熔体中f(O₂)升高,而不是降低。李延河等(2020)认为在高氧化性成矿岩浆中,硫主要以SO₄²⁻形式存在,而不是SO₂,SO₂是高度不稳定的活性气体组分,会不断与周围其他组分反应直至稳定态,因此SO₂不能长时间、大范围存在于岩浆熔体中,可能只是SO₄²⁻还原或S²⁻氧化的一个中间产物。③SO₂的歧化反应:传统观点认为从岩浆中分离出的岩浆热液与岩浆具有类似的高氧化性,当系统温度冷却至450°C时,热液中SO₂发生歧化反应,生成H₂S和H₂SO₄(式(1)),二者分别与Fe、Mo和Ca

等元素结合形成金属硫化物和石膏沉淀(Kusakabe et al., 2000; Simon et al., 2011; Hedenquist et al., 2013; Richards, 2015)。如果SO₂歧化反应是向成矿系统提供还原硫的主要方式,则矿床中形成硬石膏的量应远大于硫化物的量,这与实际情况不符,因此SO₂歧化反应可能是向成矿系统提供还原硫S²⁻的途径之一,但可能不是主要的。



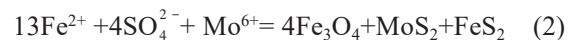
以上3种观点均认为斑岩岩浆-热液成矿系统氧化还原状态的转变是系统自身演化的结果,是一个渐变过程。实际上1个大型高品位热液矿床的形成,不仅需要丰富的成矿物质,而且要求成矿物质高效卸载富集机制,以上3种机制均不能使成矿物质高效卸载富集,容易造成成矿物质分散,故不能作为形成大矿富矿的主要途径。

2.2 围岩中还原组分加入是成矿系统氧化-还原状态转变的关键

围岩在斑岩钼(铜)矿成矿中的作用长期被忽视,实际上,围岩在斑岩钼(铜)矿成矿过程中发挥了极其重要的作用,很多斑岩钼(铜)矿床、矿体的分布和矿石品位明显受特定的围岩地层、岩性控制,有些矿体直接产在围岩中、围岩-岩体接触带,如美国Mt. Emmons (Thomas et al., 1982)、智利El Teniente (Cannell et al., 2005; Stern et al., 2007)、蒙古国Oyu Tolgoi (Perello et al., 2001)、中国南泥湖-三道庄-上房沟(叶会寿等,2006a)斑岩钼/铜矿等。

围岩中还原组分多种多样,但常见的能使斑岩成矿系统氧化-还原状态发生重大转变的还原组分主要有2种:还原性富亚铁(Fe²⁺)围岩和还原性富碳质围岩。

(1)还原性富亚铁(Fe²⁺)围岩。围岩中Fe²⁺能够将高氧化性成矿岩浆热液流体中SO₄²⁻有效还原为S²⁻,围岩中部分Fe²⁺自身被氧化形成磁铁矿/赤铁矿沉淀,S²⁻与未氧化Fe²⁺和Mo⁴⁺结合形成黄铁矿和辉钼矿等金属硫化物沉淀(李延河等,2013; 2014; Duan et al., 2021; Guo et al., 2022; 2023)(式(2))。



在南美火山岩地区的斑岩铜钼矿,富含亚铁的岩石主要为安山岩-玄武岩等中基性火山岩(Cannell et al., 2005; Stern et al., 2007),智利El Teniente斑岩铜钼矿围岩为辉长岩-辉绿岩-玄武岩杂岩(Skewes et al., 2003; Vry et al., 2010),蒙古国Oyu Tolgoi斑岩铜钼矿为拉斑玄武岩系列(Perello et al., 2001)。中国

秦岭-大别钼矿带,以安山-玄武质火山岩为斑岩钼矿围岩的情况也非常普遍,如金堆城钼矿、东沟钼矿均产在成矿花岗斑岩与熊耳群安山岩、玄武安山岩的内外接触带(杨永飞等,2011; Xu et al., 2023)。这些富亚铁的火山岩为氧化性斑岩成矿系统提供了大量 Fe^{2+} 作为还原剂,使 SO_4^{2-} 快速还原, Fe^{2+} 被氧化形成磁铁矿等铁氧化物,同时铁钼铜等金属硫化物高效沉淀富集,在成矿斑岩与铁镁质岩石的接触带部位形成高品位钼矿,过量的 SO_4^{2-} 形成石膏、重晶石等硫酸盐矿物。

(2) 还原性碳质围岩。Rowins (2000) 研究发现尽管绝大部分斑岩铜矿是高氧化性的,但也有部分显示还原性特征,这些还原性斑岩铜(金)矿床缺乏原生赤铁矿、磁铁矿和石膏等硫酸盐矿物,含有丰富的岩浆成因磁黄铁矿,成矿流体中含有大量 CH_4 等还原性气体。近年来研究发现部分斑岩钼矿也具有上述还原性特征,并将其命名为还原性钼矿床(曹冲,2018),如新疆的苏云河、宏远、白山钼矿床等。Rowins (2000)认为这些还原性斑岩铜(金)矿与氧化性斑岩铜矿一样,初始母岩浆也是氧化的,只是后来在岩浆上升过程中同化混染了含石墨的还原性地层,进而转变为还原性斑岩(Ague et al., 1988; Wilkinson, 2013)。还原性斑岩钼矿只是碳质围岩影响斑岩成矿的一个特例,不是本研究的主要内容。实际上含碳质地层分布广泛,还原性碳质围岩的加入不仅发生在岩浆阶段,更多、更普遍地发生在热液成矿阶段,这些将在下文进行讨论。

2.3 甲烷是碳质围岩向成矿系统提供的重要还原剂

碳质围岩不仅可以向斑岩成矿系统提供碳质还原剂,还可以提供甲烷等气体还原剂。甲烷等是地层中有机质热分解产生的主要气体,也是热液与碳质反应的重要产物($2\text{C}+2\text{H}_2\text{O}=\text{CH}_4+\text{CO}_2$)(Andersen et al., 1996; Fan et al., 2004),是斑岩铜-钼矿流体包裹体中最主要的还原性气体成分,如南泥湖-三道庄-上房沟、沙坪沟斑岩钼矿主成矿期矿物流体包裹体中均含 CH_4 、 CO 等还原性气体组分(图 9a-d)(刘孝善等,1987; Yang et al., 2013),指示 CH_4 参与了斑岩钼矿的形成。Climax, Urad-Henderson 和 Mt. Emmons 等超大型钼矿床附近 Mesaverde 组和 Wasatch 组中发现大量可开采的天然气(Drake et al., 2019)。

甲烷还原性强,迁移速度快,迁移距离远,而且无需碳质围岩与岩体直接接触,就可以沿成矿构造裂隙向成矿系统提供还原剂(李延河等,2020)。在

岩浆热液活动过程中,随着热液的不断累积,围岩发生超压爆裂,形成网脉状构造裂隙和角砾岩,流体压力骤降,发生减压沸腾,岩浆热液由岩浆系统进入围岩;同时围岩地层中有机质受热分解和或碳质与热液反应产生甲烷等还原性气体,并随加热循环的大气降水热液沿成矿裂隙快速由围岩扩散至斑岩岩浆-热液成矿系统,在成矿斑岩体内、斑岩体与围岩的接触带,与高温、高氧化性岩浆热液混合,引发 SO_4^{2-} 快速还原形成 S^{2-} , S^{2-} 与 Fe^{2+} 、 Mo^{4+} 等结合形成辉钼矿等金属硫化物高效沉淀富集,以微细网脉形式充填于裂隙系统,发生大规模钼矿化。同时 CH_4 被氧化形成 CO_2 (式(3)),成矿流体中 CO_2 大量富集,围岩多发生碳酸盐化(青磐岩化)。



南泥湖-三道庄-上房沟斑岩-矽卡岩型钨钼矿床中热液方解石的 $\delta^{13}\text{C}_{\text{V-PDB}}$ 值异常低,变化范围 $-9.1\text{\textperthousand} \sim -1.6\text{\textperthousand}$,平均 $-5.9\text{\textperthousand}$,与三川组沉积碳酸盐岩围岩的碳同位素组成(2.0%~2.3%)明显不同(图 10)(刘孝善等,1987,向君峰,2012; Yang et al., 2017)。曹四夭斑岩钼矿床早期阶段石英流体包裹体的 $\delta^{13}\text{C}_{\text{V-PDB}}$ 值异常低, $-16.5\text{\textperthousand} \sim -8.8\text{\textperthousand}$,平均 $-12.8\text{\textperthousand}$,中间阶段流体包裹体的 $\delta^{13}\text{C}_{\text{V-PDB}}$ 值为 $-9.3\text{\textperthousand}$,晚阶段流体包裹体的 $\delta^{13}\text{C}_{\text{V-PDB}}$ 值为 $-11.4\text{\textperthousand} \sim -5.3\text{\textperthousand}$,平均 $-7.7\text{\textperthousand}$,与海相沉积碳酸盐岩和深源岩浆的碳同位素组成明显不同,而与有机碳同位素相似(Hoefs, 2015; Wang et al., 2017),指示成矿系统中的碳可能来自集宁群黄土窑岩组围岩中的石墨及其热解产生的甲烷。沙坪沟钼矿中含辉钼矿石英脉中流体包裹体的 $\delta^{13}\text{C}_{\text{V-PDB}}$ 值为 $-4.9\text{\textperthousand}$,位于沙坪沟钼矿外围,与沙坪沟钼矿属于同一斑岩成矿系统的银母寺 Pb-Zn 矿中石英流体包裹体的 $\delta^{13}\text{C}_{\text{V-PDB}}$ 值更低, $-25.8\text{\textperthousand} \sim -9.2\text{\textperthousand}$,平均 $-17.7\text{\textperthousand}$ (吴皓然等,2019),指示庐镇关群仙人冲组富含石墨的围岩向成矿系统提供了甲烷等还原剂。这些结果为碳质围岩参与斑岩矿化提供了可靠的证据。

总之,含碳质围岩是斑岩成矿的重要条件,甲烷等还原性气体加入是引起氧化性斑岩成矿系统氧化还原状态转变的理想还原剂。

2.4 碳质围岩中还原组分加入的时机

碳质围岩中还原组分的加入,不仅发生在岩浆阶段,更普遍地发生在热液阶段。

(1) 岩浆阶段:围岩中还原组分在成矿岩浆侵位过程中加入。高氧化性成矿斑岩在上侵过程中,在

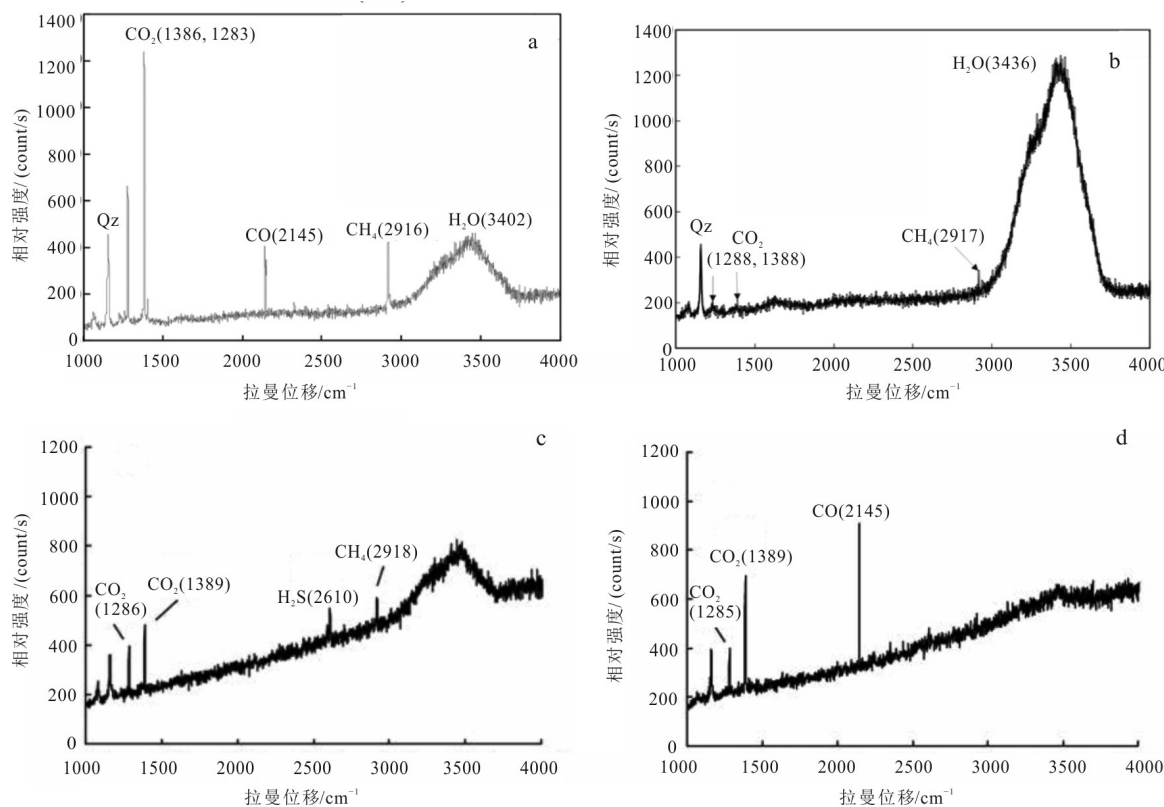


图9 南泥湖-三道庄-上房沟斑岩型钼矿床流体包裹体激光拉曼图谱

a、b. 上房沟钼矿床石英包裹体含 CH_4 、 CO 等还原气体组分 (Yang et al., 2013); c、d. 南泥湖-三道庄钼矿床 C 型包裹体中含 CH_4 、 H_2S 、 CO 等气体组分(石英霞等, 2009)

Fig.9 Laser Raman spectra of fluid inclusions of the Nannihu-Sandaozhuang-Shangfanggou porphyry Mo deposits

a, b. Reductive components such as CH_4 and CO of fluid inclusions in quartz of the Shangfanggou Mo deposit (Yang et al., 2013); c, d. Gas components such as CH_4 , H_2S and CO of C-type inclusions of the Nannihu-Sandaozhuang W-Mo deposit (Shi et al., 2009)

岩浆房与富碳质围岩发生同化混染,使成矿岩浆的氧逸度大幅降低,形成所谓的还原性斑岩(Rowins, 2000)。碳质还原组分在岩浆阶段加入将导致成矿岩浆中 SO_4^{2-} 过早还原生成金属硫化物,不利于钼、硫等成矿物质从熔体中全部转移出来,造成钼、硫等成矿物质分散,难以形成大矿、富矿(Gao et al., 2020)。

(2)热液阶段:围岩中的还原组分在成矿岩浆侵位之后的热液阶段加入,可进一步分为2种情况:①碳质围岩碳质含量高,规模大(形成石墨矿),产生的甲烷数量多、浓度高,甲烷等还原剂沿成矿裂隙大规模快速扩散至成矿斑岩之中,与氧化性成矿流体混合,使热液中 SO_4^{2-} 全部还原,形成金属硫化物沉淀富集,矿体主要产在斑岩体内及早阶段形成的杂岩体中,如沙坪沟钼矿(陆三明等,2019)、鱼池岭钼矿(李诺等,2009;周柯等,2009);②围岩中碳质含量低,规模小,提供的甲烷数量少,浓度低,不足以将斑岩体内溶液中硫酸盐全部还原沉淀。剩余未还原的氧

化性成矿热液沿构造裂隙从斑岩体中迁出进入围岩地层之中,继续与地层中的 C、 CH_4 等还原剂反应,形成辉钼矿等金属硫化物沉淀,矿体多分布在岩体与围岩的内外接触带或围岩之中,矿体明显受含碳地层控制,如南泥湖-三道庄-上房沟钼矿(Yang et al., 2013; 2017)。因此以甲烷为还原剂时,矿化不仅发生在岩体-围岩的内外接触带,也发生在斑岩体内部。

2.5 高氧化性岩浆+还原性碳质围岩/富亚铁围岩是评价斑岩钼(铜)成矿的有效新指标

高氧逸度岩浆是公认的评价斑岩成矿的有效指标,高氧化性岩浆-热液成矿系统有利于铜-钼、硫等成矿物质从熔体转移至流体,形成高浓度成矿溶液。但并非所有的高氧化性斑岩都成矿,成矿还需要围岩提供还原组分将高氧化性成矿流体中的 SO_4^{2-} 还原,使钼等成矿物质以辉钼矿等硫化物的形式快速沉淀、高效富集。在中国大型斑岩钼矿的围岩中普遍存在暗色-黑色还原性含碳质砂板岩、千枚岩、碳

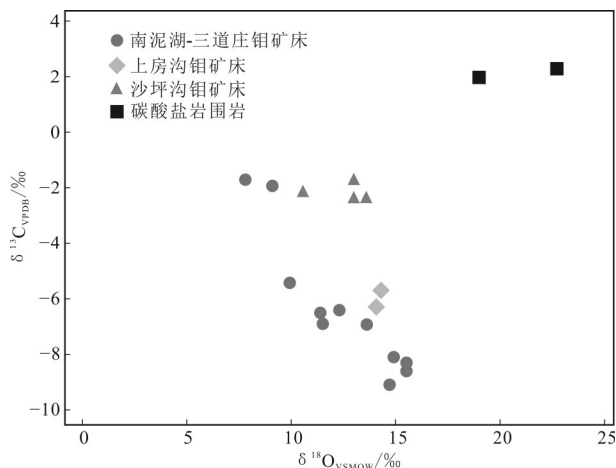


图10 沙坪沟钼矿、南泥湖-三道庄-上房沟钼矿床和围岩碳氧同位素组成(据刘孝善等,1987;向君峰等,2012;Yang et al., 2017;Guo et al., 2023)

Fig.10 Carbon and oxygen isotopic compositions of calcite from the Shapinggou Mo deposit, the Nannihu-Sandaozhuang-Shangfanggou porphyry W-Mo deposits, and surrounding marine carbonate (data are from Liu et al., 1987; Xiang et al., 2012; Yang et al., 2017; Guo et al., 2023)

酸盐岩等,这些黑色岩系不仅可以为氧化性斑岩成矿系统提供还原剂,自身还是优质的天然隔水层,是斑岩成矿的重要条件。甲烷等是地层中有机质热分解和碳质与热液反应产生的主要气体产物,还原性强,迁移能力强,可以扩散进入斑岩体内,是斑岩热液成矿系统理想的还原剂。含碳质围岩等还原组分的加入是造成高氧化性成矿流体还原、矿质卸载沉淀的关键因素之一。因此,高氧化性斑岩+还原性碳质围岩/富亚铁围岩是评价斑岩成矿的有效新指标。

值得注意的是,由于岩体侵入和构造抬升,可导致矿区地壳隆升,还原性含碳质围岩可能被剥蚀不见或残缺不全,但矿区外围仍可能保留了该套地层。因此斑岩铜-钼矿区内部及其外围沉积地层中是否发育含石墨矿/石煤、黑色碳质泥-砂岩、黑色碳质灰岩、天然气等还原性组分的沉积建造及富含亚铁的中-基性火山岩,是找寻斑岩铜-钼矿的重要依据,为找寻斑岩型铜-钼矿提供了新思路。

3 结 论

(1) 高氧逸度岩浆是斑岩钼(铜)矿成矿的必要条件,围岩中还原组分加入是触发斑岩成矿系统氧

化-还原状态转变和矿质卸载成矿的关键。黑色富碳质围岩和富铁中-基性火山岩是2种最常见的引发氧化性斑岩成矿系统还原成矿的围岩类型。

(2) 典型大型斑岩钼矿围岩或附近地层中普遍发育黑色含碳质地层,在成矿过程中普遍发生褪色蚀变,流体包裹体普遍含有甲烷等还原性气体组分,蚀变围岩和矿床中方解石及矿物流体包裹体的δ¹³C值异常低,与海相碳酸盐岩围岩显著不同。

(3) 甲烷等还原性气体是碳质围岩向斑岩成矿系统提供的主要还原剂,CH₄等沿构造裂隙扩散进入斑岩成矿系统,无需斑岩与围岩直接接触就能将成矿系统还原:如围岩碳质含量高,产生甲烷数量大,能够将成矿溶液中SO₄²⁻在斑岩体内全部还原,则矿体主要产在斑岩体内;如围岩碳质含量低,产生甲烷数量不足,矿体主要赋存于斑岩体与围岩的内外接触带。

(4) 高氧化性斑岩岩浆+还原性碳质围岩/富亚铁围岩是高效评价斑岩铜-钼成矿的新指标。

致 谢 在野外工作中得到了安徽省地质矿产勘查局313地质队王波华、方明高工的大力支持和帮助,两位审稿人提出建设性修改意见和建议,在此表示一并表示感谢!

References

- Ague J J and Brimhall G H. 1988. Magmatic arc asymmetry and distribution of anomalous plutonic belts in the Batholiths of California: Effects of assimilation, crustal thickness, and depth of crystallization[J]. Geological Society of America Bulletin, 100: 912-927.
- Andersen T and Burke E A J. 1996. Methane inclusions in shocked quartz from the Gardnos impact breccia, South Norway[J]. European Journal of Mineralogy, 8: 927-936.
- Audétat A. 2015. Compositional evolution and formation conditions of magmas and fluids related to porphyry Mo mineralization at Climax, Colorado[J]. Journal of Petrology, 56: 1519-1546.
- Audétat A and Li W. 2017. The genesis of Climax-type porphyry Mo deposits: Insights from fluid inclusions and melt inclusions[J]. Ore Geology Reviews, 88: 436-460.
- Ballard J R, Palin M J and Campbell I H. 2002. Relative oxidation states of magmas inferred from Ce(IV)/Ce(III) in zircon: Application to porphyry copper deposits of northern Chile[J]. Contribution Mineral Petrology, 144: 347-364.
- Burnham A D and Berry A J. 2012. An experimental study of trace element partitioning between zircon and melt as a function of oxygen fugacity[J]. Geochimica et Cosmochimica Acta, 95: 196-212.

- Cannell J, Cooke D R, Walshe J L and Stein H. 2005. Geology, mineralization, alteration, and structural evolution of the El Teniente porphyry Cu-Mo deposit[J]. In Econ. Geol. and the Bulletin of the Society of Economic Geologists; The Economic Geology Publishing Company: Littleton, CO, USA, 100: 979-1003.
- Cao C and Shen P. 2018. Advances and problems in study of porphyry molybdenum deposits[J]. Geological Review, 64(2): 477-497(in Chinese with English abstract).
- Carten R B, White W H and Stein H J. 1993. High-grade granite-related molybdenum systems: Classification and origin[J]. Mineral deposit modeling: Geological Association of Canada Special Paper, 40: 521-554.
- Chen Y J, Li N and Deng X H. 2020. Molybdenum mineralization in Qinling Orogeny[M]. Beijing, China: Science Press. 1-858(in Chinese).
- Clark K F. 1972. Stockwork molybdenum deposits in the western Cordillera of North America[J]. Econ. Geol., 67: 731-758.
- Collins B A. 2020. Geology of the coal-bearing Mesaverde Formation (Cretaceous), coal basin area, Pitkin Country, Colorado[D]. Supervisor: Grose L T. Colorado School of Mines, Golden, CO, USA, 1-116.
- Donnell J R. 1961. Tertiary geology and oil-shale resources of the Piceance Creek Basin between the Colorado and White Rivers, northwestern Colorado, U.S[R]. Geological Survey: Bulletin, WA, USA, 835-891.
- Duan C, Li Y, Mao J, Zhu Q, Xie G, Wan Q, Jian W and Hou K. 2021. The role of evaporite layers in the ore-forming processes of iron oxide-apatite and skarn Fe deposits: Examples from the Middle-Lower Yangtze River Metallogenic Belt, East China[J]. Ore Geology Review, 138: 104352.
- Drake R M I I, Schenck C J, Mercier T J, Le P A, Finn T M, Johnson R C, Woodall C A, Gaswirth S B, Marra K R and Pitman J K. 2019. Assessment of undiscovered continuous tight-gas resources in the Mesaverde Group and Wasatch Formation, Uinta-Piceance Province, Utah and Colorado, 2018[J]. USGS Fact Sheet; U.S. Geological Survey: Reston, VA, USA, 1-2.
- Fan H R, Xie Y H, Wang K Y and Wilde S A. 2004. Methane-rich fluid inclusions in skarn near the giant REE-Nb-Fe deposit at Bayan Obo, Northern China[J]. Ore Geology Reviews, 25: 301-309.
- Fan H Y, Li T G, Wu W H, Zhang M Y, Huang F, Zhao Z, Zhang T, Xu L Q, Li X Z and Quan Z X. 2018. Chronology of giant Caosiyao porphyry Mo-Pb-Zn-Au ore-forming system and their geological significance in Xinghe County, Central Inner Mongolia[J]. Mineral Deposits, 37 (2): 355-370(in Chinese with English abstract).
- Gao Y, Yang Y C, Han S J and Meng F. 2020. Geochemistry of zircon and apatite from the Mo ore-forming granites in the Dabie Mo belt, East China: Implications for petrogenesis and mineralization[J]. Ore Geology Reviews, 126: 103733.
- Guo B, Zhu L M, Li B, Xu J, Wang J Q and Gong H J. 2009. Isotopic and element geochemical study of Jinduicheng superlarge porphyry Mo deposit in East Qinling area[J]. Mineral Deposits, 28(3): 265-281(in Chinese with English abstract).
- Guo D, Li Y, Duan C and Fan C. 2022. Involvement of evaporite layers in the formation of iron oxide-apatite ore deposits: Examples from the Luohe deposit in China and the El Laco deposit in Chile[J]. Minerals, 12: 1043.
- Guo D, Li Y, Duan C, Fan C and Sun P. 2023. The role of reductive carbonaceous surrounding rocks in the formation of porphyry Mo deposits[J]. Minerals, 13(7): 951.
- He J, Xu X C, Xie Q Q, Fan Z L and Chen T H. 2016. Evidence from pseudomorphous-quartz phenocryst for decompression of rock-forming and ore-forming processes in Shapinggou porphyry Mo deposit[J]. Science China Earth Sciences, 59: 1014-1024(in Chinese with English abstract).
- Hedenquist J W and Taran Y A. 2013. Modeling the formation of advanced argillic lithocaps: Volcanic vapor condensation above porphyry intrusions[J]. Econ. Geol., 108: 1523-1540.
- Heintze L. 1985. Geology and geochemistry of the porphyry stockwork molybdenum deposit at Tamboras, La Negra Zone (Peru)[J]. Econ. Geol., 80: 2019-2027.
- Hoefs J. 2015. Stable isotope Geochemistry[M]. Seventh edition. Berlin: Springer Verlag. 1-383.
- Huang D H, Wu C Y, Du A D and He H L. 1994. Re-Os isotope ages of molybdenum deposits in East Qinling and their significance[J]. Mineral Deposits, 13(3): 221-230(in Chinese with English abstract).
- Jiang Z, Shang L, Guo H, Wang X, Chen C and Zhou Y. 2021. An experimental investigation into the partition of Mo between aqueous fluids and felsic melts: Implications for the genesis of porphyry Mo ore deposits[J]. Ore Geology Reviews, 134: 104144.
- Kelley K A and Cottrell E. 2012. The influence of magmatic differentiation on the oxidation state of Fe in a basaltic arc magma[J]. Earth and Planetary Science Letters, 329-330: 109-121.
- Kusakabe M, Komoda Y, Takano B and Abiko T. 2000. Sulfur isotopic effects in the disproportionation reaction of sulfur dioxide in hydrothermal fluids: Implications for the $\delta^{34}\text{S}$ variations of dissolved bisulfate and elemental sulfur from active crater lakes[J]. Journal of Volcanology and Geothermal Research, 97: 287-307.
- Lawley C J M, Richards J P, Anderson R G, Creaser R A and Heaman L M. 2010. Geochronology and geochemistry of the max porphyry Mo deposit and its relationship to Pb-Zn-Ag mineralization, Kootenay Arc, Southeastern British Columbia, Canada[J]. Econ. Geol., 105: 1113-1142.
- Li N, Chen Y J, Ni Z Y and Hu H Z. 2009. Characteristics of ore-forming fluids of the Yuchiling porphyry Mo deposit, Songxian County, Henan province, and its geological significance[J]. Acta Petrologica Sinica, 25(10): 2509-2522(in Chinese with English abstract).
- Li Y F, Mao J W, Hu H B, Guo B J and Bai F J. 2005. Geology, distribution, types and tectonic settings of Mesozoic molybdenum deposits in East Qinling area[J]. Mineral Deposits, 24(3): 292-304 (in Chinese with English abstract).
- Li Y H, Xie G Q, Duan C and Han D. 2013. Effect of sulfate evaporate

- salt layer over the formation of skarn-type iron ores[J]. *Acta Geologica Sinica*, 87: 1324-1334(in Chinese with English abstract).
- Li Y H, Duan C, Han D, Chen X W, Wang C L, Yang B Y, Zhang C and Liu F. 2014. Effect of sulfate evaporate salt layer for formation of porphyrite iron ores in the Middle-Lower Yangtze River area[J]. *Acta Petrologica Sinica*, 30 (5): 1355-1368(in Chinese with English abstract).
- Li Y H, Duan C, Zeng P S, Jian W, Wan Q, Hu G Y, Zhao X Y and Wu X P. 2020. The role of reductive carbonaceous strata in the formation of porphyry copper ores[J]. *Acta Geoscientica Sinica*, 41(5): 637-650(in Chinese with English abstract).
- Li Z and Schieber J. 2018. Composite particles in mudstones: Examples from the late Cretaceous Tununk Shale Member of the Manacos Shale Formation[J]. *Journal of Sedimentary Research*, 88: 1319-1344.
- Linnen R L and Williams-Jones A E. 1990. Evolution of aqueous-carbonic fluids during contact metamorphism, wall-rock alteration, and molybdenite deposition at Trout Lake, British Columbia[J]. *Econ. Geol.*, 85: 1840-1856.
- Liu X S, Wu C Y and Huang B. 1987. Origin and evolution of the hydrothermal system in Nannihu-Sandaozhuang molybdenum (tungsten) ore deposit, Luanchuan country, Henan Province[J]. *Geochimica*, 3: 199-207(in Chinese with English abstract).
- Lorenz J C and Nadon G C. 2002. Braided-river deposits in a muddy depositional setting: The Molina Member of the Wasatch Formation (Paleogene), west-central Colorado, U S A[J]. *Journal of Sedimentary Research*, 72: 376-385.
- Lu S M, Li J S, Ruan L S, Zhao L L, Huang F, Wang B H and Zhang H D. 2019. The characteristics of stable isotope geochemistry of Shapinggou molybdenum deposit, Anhui Province[J]. *Geoscience*, 33(2): 262-270(in Chinese with English abstract).
- Ludington S and Plumlee G S. 2009. Climax-type porphyry molybdenum deposits[R]. US geological survey, open-file report., 1215(16).
- Mao J W, Hua R M and Li X B. 1999. A preliminary study of large-scale metallogenesis and large clusters of mineral deposits[J]. *Mineral Deposits*, 18(4): 291-299(in Chinese with English abstract).
- Mao J W, Pirajno F, Xiang J F, Gao J J, Ye H S, Li Y F and Guo B J. 2011. Mesozoic molybdenum deposits in the east Qinling-Dabie orogenic belt: Characteristics and tectonic settings[J]. *Ore Geology Reviews*, 43: 264-293.
- Muñoz M, Charrier R, Fanning C M, Maksae V and Deckart K. 2012. Zircon trace element and O-Hf isotope analyses of mineralized intrusions from El Teniente ore deposit, Chilean Andes: Constraints on the source and magmatic evolution of porphyry Cu-Mo related magmas[J]. *Journal of Petrology*, 53: 1091-1122.
- Ouyang H, Mao J and Hu R. 2020. Geochemistry and crystallization conditions of magmas related to porphyry Mo mineralization in Northeastern China[J]. *Econ. Geol.*, 115: 79-100.
- Ouyang H, Mao J, Hu R, Caulfield J and Zhou Z. 2021. Controls on the metal endowment of porphyry Mo deposits: Insights from the Luming porphyry Mo deposits, northeastern China[J]. *Econ. Geol.*, 116: 1711-1735.
- Ouyang H, Caulfield J, Mao J and Hu R. 2022. Controls on the formation of porphyry Mo deposits: insights from porphyry (-skarn) Mo deposits in Northeastern China[J]. *American Mineralogist*, 107: 1736-1751.
- Perello J, Cox D, Garamjav D, Sanjdorj S, Diakov S, Schissel D, Munkhbat T and Oyun G. 2001. Oyu Tolgoi, Mongolia; Siluro-Devonian porphyry Cu-Au-(Mo) and high-sulfidation Cu mineralization with a Cretaceous chalcocite blanket[J]. *Econ. Geol.*, 96: 1407-1428.
- Ren Z, Zhou T F, Yuan F and Zhang H D. 2020. Characteristics of the metallogenetic system of the Shapinggou super-large porphyry molybdenum deposit in the Dabie orogenic belt, Anhui Province[J]. *Earth Science Frontiers*, 27: 353-372(in Chinese with English abstract).
- Richards J P. 2015. The oxidation state, and sulfur and Cu contents of arc magmas: Implications for metallogeny[J]. *Lithos*, 233: 27-45.
- Roedder E. 1971. Fluid inclusion studies on the porphyry-type ore deposits at Bingham, Utah, Butte, Montana, and Climax, Colorado[J]. *Econ. Geol.*, 66: 98-118.
- Roehler H W. 1979. Vermillion Creek coal bed, high-sulfur, radioactive coal of paludal-lacustrine origin in Wasatch Formation of Vermillion Creek basin, Wyoming and Colorado[J]. *AAPG Bulletin*, 63: 839.
- Roehler HW and Martin P L. 1987. Geological investigations of the Vermillion Creek coal bed in the Eocene Niland Tongue of the Wasatch Formation, Sweetwater County, Wyoming[R]. U.S. Geological Survey Professional Papers; U.S. Geological Survey: Denver, CO, USA. 1314.
- Rowins S M. 2000. Reduced porphyry copper-gold deposits: A New variation on an old theme[J]. *Geology*, 28: 491-494.
- Sanchez J D. 1990. Stratigraphic framework, coal zone correlations, and depositional environment of the upper Cretaceous Blackhawk Formation and star point sandstone in the Scofield and Beaver Creek Areas, Nephi 30' x 60' quadrangle, Wasatch Plateau coal field, Carbon County, Utah[R]. Coal Investigations Map; U. S. Geological Survey: Reston, VA, USA.
- Seedorff E. 2004a. Henderson porphyry molybdenum system, Colorado: I. Sequence and abundance of hydrothermal mineral assemblages, flow paths of evolving fluids, and evolutionary style[J]. *Econ. Geol.*, 99(1): 3-37.
- Seedorff E. 2004b. Henderson porphyry molybdenum system, Colorado: II. Decoupling of introduction and deposition of metals during geochemical evolution of hydrothermal fluids[J]. *Econ. Geol.*, 99 (1): 37-72.
- Selby D, Nesbitt B E, Muehlenbachs K and Prochaska W. 2000. Hydrothermal alteration and fluid chemistry of the Endako porphyry molybdenum deposit, British Columbia[J]. *Econ. Geol.*, 95: 183-202.
- Shi Y X, Li N and Yang Y. 2009. Ore geology and fluid inclusion geo-

- chemistry of the Sandaozhuang Mo-W deposit in Luanchuan County, Henan Province[J]. *Acta Petrologica Sinica*, 25(10): 2575-2587(in Chinese with English abstract).
- Sillitoe R H. 1980. Types of porphyry molybdenum deposits[J]. *Mining Magazine*, 142(6): 550-553.
- Sillitoe R H and Thompson J F H. 1998. Intrusion-related vein gold deposits: Types, tectono-magmatic settings and difficulties of distinction from orogenic gold deposits[J]. *Resource Geology*, 48: 237-250.
- Sillitoe R H. 2010. Porphyry copper systems[J]. *Econ. Geol.*, 105: 3-41.
- Simon A C and Ripley E M. 2011. The role of magmatic sulfur in the formation of ore deposits[J]. *Reviews in Mineralogy and Geochemistry*, 73: 513-578.
- Skewes M A, Holmgren C and Stern C R. 2003. The Donoso copper-rich, tourmaline-bearing breccia pipe in central Chile: Petrologic, fluid inclusion and stable isotope evidence for an origin from magmatic fluids[J]. *Mineralium Deposita*, 38: 2-21.
- Stern C R, Funk J A, Skewes M A and Arevalo A. 2007. Magmatic anhydrite in plutonic rocks at the El Teniente Cu-Mo deposit, Chile, and the role of sulfur- and copper-rich magmas in its formation[J]. *Econ. Geol.*, 102: 1335-1344.
- Sun W, Liang H, Ling M, Zhan M, Ding X, Zhang H, Yang X, Li Y, Ireland T R and Wei Q. 2013. The link between reduced porphyry copper deposits and oxidized magmas[J]. *Geochimica et Cosmochimica Acta*, 103: 263-275.
- Sun W, Huang R, Li H, Hu Y, Zhang C, Sun S, Zhang L, Ding X, Li C, Zartman R E and Ling M. 2015. Porphyry deposits and oxidized Magmas[J]. *Ore Geology Reviews*, 65: 97-131.
- The Second Geological Exploration Institute of Henan Province Bureau of Geology and Mineral Resources. 2014. Report of Caoshiyao molybdenum deposit in Xinghe County, Inner Mongolia Autonomous Region[R]. 1-146(in Chinese).
- Thomas J A and Galey J T. 1982. Exploration and geology of the Mt. Emmons molybdenite deposits, Gunnison County, Colorado[J]. *Econ. Geol.*, 77: 1085-1104.
- Thompson J F H, Sillitoe R H, Baker T, Lang J R and Mortensen J K. 1999. Intrusion-related gold deposits associated with tungsten-tin Provinces[J]. *Mineralium Deposita*, 34: 323-334.
- Trail D, Bruce W E and Tailby N D. 2012. Ce and Eu anomalies in zircon as proxies for the oxidation state of magmas[J]. *Geochimica et Cosmochimica Acta*, 97: 70-87.
- U.S. Geological Survey. 2023. USGS Mineral Commodity Summaries [R]. U.S. Geological Survey: Reston, VA, USA. 2023.
- Vigneresse J L, Truche L and Richard A. 2019. How do metals escape from magmas to form porphyry-type ore deposits[J]? *Ore Geology Reviews*, 105: 310-336.
- Vry V H, Wilkinson J J, Seguel J and Millan J. 2010. Multistage intrusion, brecciation, and veining at El Teniente, Chile: Evolution of a nested porphyry system[J]. *Econ. Geol.*, 105: 119-153.
- Wang G R, Wu G, Xu L Q, Li X Z, Zhang T, Quan Z X, Wu H, Li T G, Liu J and Chen Y C. 2017. Molybdenite Re-Os age, H-O-C-S-Pb isotopes, and fluid inclusion study of the Caoshiyao porphyry Mo deposit in Inner Mongolia, China[J]. *Ore Geology Reviews*, 81: 728-744.
- Wang S. 1989. Characteristics of ore-bearing formation and genesis of the Xinghe graphite deposit in Inner Mongolia[J]. *Mineral Deposits*, 8(1): 85-96(in Chinese with English abstract).
- Wang X X, Li Y F, Li H Y, Ke C H, Wang X Y and Li J B. 2015. Jinduicheng porphyry molybdenum deposit in Shanxi Province[M]. Beijing: Geological Press. 1-153(in Chinese).
- Wilkinson J J. 2013. Triggers for the formation of porphyry ore deposits in magmatic arcs[J]. *Nature Geoscience*, 6: 917-925.
- Wu G, Li X Z, Xu L Q, Wang G R, Liu J, Zhang T, Quan Z X, Wu H, Li T G, Zeng Q T and Chen Y C. 2017. Age, geochemistry, and Sr-Nd-Hf-Pb isotopes of the Caoshiyao porphyry Mo deposit in Inner Mongolia, China[J]. *Ore Geology Reviews*, 81(2): 706-727.
- Wu H R, Xie Y L, Zhong R C, Wang Y and An W J. 2019. Geology, fluid inclusion and stable isotopes of the Yinshuisi Zn-Pb deposit, Jinzhai County, Anhui Province[J]. *Geotectonica et Metallogenesis*, 43: 967-990(in Chinese with English abstract).
- Wu H Y, Zhang L C, Pirajno F, Shu Q H, Zhang M, Zhu M T and Xiang P. 2016. The Mesozoic Caoshiyao giant porphyry Mo deposit in Inner Mongolia, North China and Paleo-Pacific subduction-related magmatism in the northern North China Craton[J]. *Journal of Asian Earth Sciences*, 127: 281-299.
- Xiang J F, Pei R F, Ye H S, Wang C Y and Tian Z H. 2012. Source and evolution of the ore-forming fluid in the Nannihu-Sandaozhuang Mo (W) deposit: Constraints from C-H-O stable isotope data[J]. *Geology in China*, 39(6): 1778-1789(in Chinese with English abstract).
- Xu L L, Bi X W, Zhang X C, Huang M L and Liu G. 2023. Mantle contribution to the generation of the giant Jinduicheng porphyry Mo deposit, Central China: New insights from combined in-situ element and isotope compositions of zircon and apatite[J]. *Chemical Geology*, 616: 121238.
- Yang B, Li C Y, Bo H J, Hou X H, Su P Y and Fan S H. 2023. Geochemical characteristics and genesis of Changhangou crystalline graphite deposit in Hadamengou area, Inner Mongolia[J]. *Mineral Deposits*, 42(2): 444-462(in Chinese with English abstract).
- Yang Y F, Li N and Ni Z Y. 2009a. Fluid inclusion study of the Jinduicheng porphyry Mo deposit, Hua Country, Shanxi Province [J]. *Acta Petrologica Sinica*, 25(11): 2983-2993(in Chinese with English abstract).
- Yang Y F, Li N and Yang Y. 2009b. Fluid inclusion study of the Nannihu porphyry Mo-W deposit, Luanchuan County, Henan Province[J]. *Acta Petrologica Sinica*, 25(10): 2550-2562(in Chinese with English abstract).
- Yang Y F, Li N and Wang L J. 2011. Fluid inclusion study of the Donggou porphyry Mo deposit, Henan Province[J]. *Acta Petrologica Sinica*, 27(5): 1453-1466(in Chinese with English abstract).
- Yang Y, Chen Y J, Zhang J and Zhang C. 2013. Ore geology, fluid inclusions and four-stage hydrothermal mineralization of the Shang-

- fangou giant Mo-Fe deposit in eastern Qinling, Central China[J]. Ore Geology Reviews, 55: 146-161.
- Yang Y, Liu Z J and Deng X H. 2017. Mineralization mechanisms in the Shangfanggou giant porphyry-skarn Mo-Fe deposit of the East Qinling, China: Constraints from H-O-C-S-Pb isotopes[J]. Ore Geology Reviews, 81: 535-547.
- Ye H S, Mao J W, Li Y F, Yan C H, Guo B J, Zhao C S, Zheng R F and Chen L. 2006a. Characteristics and metallogenetic mechanism of Mo W and Pb Zn-Ag deposits in Nannihu ore field western Henan Province[J]. Geoscience, 20(1): 165-174(in Chinese with English abstract).
- Ye H S, Mao J W, Li Y F, Guo B J, Zhang C Q, Liu J, Yan Q R and Liu G Y. 2006b. Shrimp zircon U-Pb and molybdenite Re-Os dating for the super-large Donggou porphyry Mo deposit in East Qinling, China and its geological implication[J]. Acta Geologica Sinica, 80 (7): 1078-1088(in Chinese with English abstract).
- Zhang D and Audébat A. 2017. Chemistry, mineralogy and crystallization conditions of porphyry Mo-forming magmas at Urad-Hendersen and Silver Creek, Colorado, USA[J]. Journal of Petrology, 58: 277-296.
- Zhang H D, Wang B H, Hao Y J, Cheng S and Xiang B. 2012. Geological characteristics and comprehensive ore-prospecting information of Shapinggou porphyry-type molybdenum deposit in Anhui Province[J]. Mineral Deposits, 31(1): 41-51(in Chinese with English abstract).
- Zhang H, Sun W D, Yang X Y, Liang H Y, Wang B H, Wang R L and Wang Y X. 2011. Geochronology and metallogenesis of the Shapinggou giant porphyry molybdenum deposit in the Dabie orogenic belt[J]. Acta Geologica Sinica, 85(12): 2039-2059(in Chinese with English abstract).
- Zhang H, Li C Y, Yang X Y, Sun Y L, Deng J H, Liang H Y, Wang R L, Wang B H, Wang Y X and Sun W D. 2014. Shapinggou: The largest Climax-type porphyry Mo deposit in China[J]. International Geology Review, 56: 313-331.
- Zhang J H, Tian H, Wang H C, Shi J R, Ren Y W, Chu H, Chang Q S, Zhong Y, Zhang K and Xiang Z Q. 2019. Re-definition of the two-stage Early-Precambrian meta-supracrustal rocks in the Huai'an complex, North China Craton: Evidences from petrology and zircon U-Pb geochronology[J]. Earth Science, 44(1): 1-22(in Chinese with English abstract).
- Zhang J, Ye H S, Shi M C and Meng F. 2013. Metallogenetic process of the Yuchiling Mo deposit in East Qinling: Constraints from fluid inclusions[J]. Geological Bulletin of China, 32(7): 1113-1128(in Chinese with English abstract).
- Zhang J, Ye H, Zhou K and Meng F. 2014. Processes of ore genesis at the world-class Yuchiling molybdenum deposit, Henan Province, China[J]. Journal of Asian Earth Sciences, 79: 666-681.
- Zhou K, Ye H S, Mao J W, Qu W J, Zhou S F, Meng F and Gao Y L. 2009. Geological characteristics and molybdenite Re-Os isotopic dating of Yuchiling porphyry Mo deposit in western Henan Province[J]. Mineral Deposits, 28(2): 170-184(in Chinese with English abstract).
- lith abstract).
- Zhou T, Zeng Q, Chu S, Zhou L and Yang Y. 2018. Magmatic oxygen fugacities of porphyry Mo deposits in the East Xing'an-Mongolian orogenic Belt (NE China) with metallogenetic implications[J]. Journal of Asian Earth Sciences, 165: 145-159.
- Zhu L M, Zhang G W, Guo B and Li B. 2008. U-Pb (LA-ICP-MS) zircon dating for the large Jinduicheng porphyry Mo deposit in the East Qinling, China, and its metallogenetic geodynamical setting[J]. Acta Geologica Sinica, 82(2): 204-220(in Chinese with English abstract).
- ### 附中文参考文献
- 曹冲, 申萍. 2018. 斑岩型钼矿床研究进展与问题[J]. 地质论评, 64 (2): 477-497.
- 陈衍景, 李诺, 邓小华. 2020. 秦岭造山带钼矿床成矿规律[M]. 北京: 科学出版社. 1-858.
- 范海洋, 李铁刚, 武文恒, 张明玉, 黄凡, 赵正, 张彤, 许立权, 李香资, 权知心. 2018. 内蒙古兴和县曹四夭超大型斑岩钼锌金成矿系统年代学及其地质意义[J]. 矿床地质, 37 (2): 355-370.
- 郭波, 朱赖民, 李彝, 许江, 王建其, 弓虎军. 2009. 东秦岭金堆城大型斑岩钼矿床同位素及元素地球化学研究[J]. 矿床地质, 28(3): 265-281.
- 何俊, 徐晓春, 谢巧勤, 范子良, 陈天虎. 2016. 安徽金寨沙坪沟斑岩矿区成岩成矿过程中的减压机制: 来自假 β 相石英的证据[J]. 中国科学: 地球科学, 46(4): 544-554.
- 河南省地质矿产勘查开发局第二地质勘查院. 2014. 内蒙古自治区兴和县曹四夭钼矿勘探报告[R]. 1-146.
- 黄典豪, 吴澄宇, 杜安道, 何红蓼. 1994. 东秦岭地区钼矿床的铼-锇同位素年龄及其意义[J]. 矿床地质, 13(3): 221-230.
- 李诺, 陈衍景, 倪智勇, 胡海珠. 2009. 河南省嵩县鱼池岭斑岩钼矿床成矿流体特征及其地质意义[J]. 岩石学报, 25(10): 2509-2522.
- 李延河, 谢桂青, 段超. 2013. 膏盐层在矽卡岩型铁矿成矿中的作用[J]. 地质学报, 87(9): 1324-1334.
- 李延河, 段超, 韩丹, 陈新旺, 王丛林, 杨秉阳, 张成, 刘锋. 2014. 膏盐层氧化障在长江中下游玢岩铁矿成矿中的作用[J]. 岩石学报, 30(5): 1355-1368.
- 李延河, 段超, 曾普胜, 简伟, 万秋, 胡吉月, 赵晓燕, 武晓珮. 2020. 还原性含碳质围岩在斑岩铜矿成矿中的作用[J]. 地球学报, 41(5): 637-650.
- 李永峰, 毛景文, 胡华斌, 郭保健, 白凤军. 2005. 东秦岭钼矿类型、特征、成矿时代及其地球动力学背景[J]. 矿床地质, 24(3): 292-304.
- 刘孝善, 吴澄宇, 黄标. 1987. 河南栾川南泥湖-三道庄钼(钨)矿床热液系统的成因与演化[J]. 地球化学, 3: 199-207.
- 陆三明, 李建设, 阮林森, 赵丽丽, 黄凡, 王波华, 张怀东. 2019. 安徽省金寨县沙坪沟钼矿床稳定同位素地球化学特征[J]. 现代地质, 33(2): 262-270.
- 毛景文, 华仁民, 李晓波. 1999. 浅议大规模成矿作用与大型矿集区[J]. 矿床地质, 18(4): 291-299.

- 任志, 周涛发, 袁峰, 张怀东. 2020. 安徽大别山地区沙坪沟超大型斑岩钼矿床成矿系统特征[J]. 地学前缘, 27(2): 353-372.
- 石英霞, 李诺, 杨艳. 2009. 河南省栾川县三道庄钼钨矿床地质和流体包裹体研究[J]. 岩石学报, 25(10): 2575-2587.
- 王时麒. 1989. 内蒙兴和石墨矿含矿建造特征与矿床成因[J]. 矿床地质, 8(1): 85-96.
- 王晓霞, 李永峰, 李洪英, 柯昌辉, 王修缘, 李金宝. 2015. 陕西金堆城斑岩钼矿[M]. 北京地质出版社. 1-153.
- 吴皓然, 谢玉玲, 钟日晨, 王莹, 安卫军. 2019. 安徽金寨银水寺铅锌矿床流体包裹体和同位素地球化学特征[J]. 大地构造与成矿学, 43(5): 967-990.
- 向君峰, 裴荣富, 叶会寿, 王春毅, 田志恒. 2012. 南泥湖-三道庄钼(钨)矿床成矿流体的碳氢氧同位素研究及其启示[J]. 中国地质, 39(6): 1778-1789.
- 杨彪, 李成元, 薄海军, 侯秀宏, 苏攀云, 樊松浩. 2023. 内蒙古哈达门沟地区长汉沟晶质石墨矿床地球化学特征与成因研究[J]. 矿床地质, 42(2): 444-462.
- 杨永飞, 李诺, 倪智勇. 2009a. 陕西省华县金堆城斑岩型钼矿床流体包裹体研究[J]. 岩石学报, 25(11): 2983-2993.
- 杨永飞, 李诺, 杨艳. 2009b. 河南省栾川南泥湖斑岩型钼钨矿床流体包裹体研究[J]. 岩石学报, 25(10): 2550-2562.
- 杨永飞, 李诺, 王莉娟. 2011. 河南省东沟超大型钼矿床流体包裹体研究[J]. 岩石学报, 27(5): 1453-1466.
- 叶会寿, 毛景文, 李永峰, 燕长海, 郭保健, 赵财胜, 何春芬, 郑榕芬, 陈莉. 2006a. 豫西南泥湖矿田钼钨及铅锌银矿床地质特征及其成矿机理探讨[J]. 现代地质, 20(1): 165-174.
- 叶会寿, 毛景文, 李永峰, 郭保健, 张长青, 刘王君, 闫全人, 刘国印. 2006b. 东秦岭东沟超大型斑岩钼矿 SHRIMP 锆石 U-Pb 和辉钼矿 Re-Os 年龄及其地质意义[J]. 地质学报, 80(7): 1078-1088.
- 张红, 孙卫东, 杨晓勇, 梁华英, 王波华, 王瑞龙, 王玉贤. 2011. 大别造山带沙坪沟特大型斑岩钼矿床年代学及成矿机理研究[J]. 地质学报, 85(12): 2039-2059.
- 张怀东, 王波华, 郝越进, 程松, 项斌. 2012. 安徽沙坪沟斑岩型钼矿床地质特征及综合找矿信息[J]. 矿床地质, 31(1): 41-51.
- 张家辉, 田辉, 王惠初, 施建荣, 任云伟, 初航, 常青松, 钟焱, 张阔, 相振群. 2019. 华北克拉通怀安杂岩中早前寒武纪两期变质表壳岩的重新厘定: 岩石学及锆石 U-Pb 年代学证据[J]. 地球科学, 44(1): 1-22.
- 张娟, 叶会寿, 史美超, 孟芳. 2013. 东秦岭鱼池岭斑岩型钼矿床成矿作用过程-来自成矿流体的约束[J]. 地质通报, 32(7): 1113-1128.
- 朱赖民, 张国伟, 郭波, 李犇. 2008. 东秦岭金堆城大型斑岩钼矿床 LA-ICP-MS 锆石 U-Pb 定年及成矿动力学背景[J]. 地质学报, 82(2): 204-220.
- 周珂, 叶会寿, 毛景文, 屈文俊, 周树峰, 孟芳, 高亚龙. 2009. 豫西鱼池岭斑岩型钼矿床地质特征及其辉钼矿铼-锇同位素年龄[J]. 矿床地质, 28(2): 170-184.